Io's Long-Wavelength Topography as a Probe for a Subsurface Magma Ocean

Szilárd Gyalay[1] and Francis Nimmo[1]

[1]University of California, Santa Cruz

November 8, 2023

Abstract

We investigate how spatial variations in tidal heating affect Io's isostatic topography at long wavelengths. The difference between the hydrostatic shape implied by Io's gravity field and its observed global shape is less than the latter's 0.3 km uncertainty. Assuming Airy isostasy, degree-2 topography <300 m amplitude is only possible if surface heat flux varies spatially by <17% of the mean value. This is consistent with Io's volcano distribution and is possible if tidal heat is generated within a convecting layer underneath the lithosphere. However, that layer would require a viscosity $<10^{10}$ Pa s. A magma ocean would have low enough viscosity but would not generate enough tidal heat internally. Conversely, assuming Pratt isostasy, we find ˜150 m degree-2 topography is easily achievable. If a magma ocean was present, Airy isostasy would dominate; we therefore conclude that Io is unlikely to possess a magma ocean.

Io's Long-Wavelength Topography as a Probe for a Subsurface Magma Ocean

S. Gyalay[1] **and F. Nimmo**[1]

[1]University of California, Santa Cruz

Key Points:

- Maximum variation in topography implies low spatial variation in Io's tidal heating when assuming Airy isostasy.
- Tidal heat produced in a convecting aesthenosphere can reduce spatial variation in tidal heating, but requires prohibitively low viscosity.
- Io's topography is consistent with expected tidal heating spatial variations if thermal expansion drives crustal density variations.

Corresponding author: Szilárd Gyalay, sgyalay@seti.org

Abstract

We investigate how spatial variations in tidal heating affect Io's isostatic topography at long wavelengths. The difference between the hydrostatic shape implied by Io's gravity field and its observed global shape is less than the latter's 0.3 km uncertainty. Assuming Airy isostasy, degree-2 topography < 300 m amplitude is only possible if surface heat flux varies spatially by $< 17\%$ of the mean value. This is consistent with Io's volcano distribution and is possible if tidal heat is generated within a convecting layer underneath the lithosphere. However, that layer would require a viscosity $< 10^{10}$ Pa s. A magma ocean would have low enough viscosity but would not generate enough tidal heat internally. Conversely, assuming Pratt isostasy, we find $\sim$150 m degree-2 topography is easily achievable. If a magma ocean was present, Airy isostasy would dominate; we therefore conclude that Io is unlikely to possess a magma ocean.

Plain Language Summary

As it orbits Jupiter elliptically, the difference in gravitational pull experienced by the moon Io results in tidal heating due to internal friction. Some evidence suggests this heat forms a magma ocean beneath Io's crust. If so, there would be a difference in the amount of heat generated at Io's equator versus its poles and would alter the thickness of Io's crust between the two locales. Assuming the crust has a uniform density, its thickness would be inversely proportional to the tidal heat beneath the crust, which in turn affects the difference in Io's radius at the equator versus at its poles. However, reasonable variation in tidal heating across Io would result in a greater difference in radius than is observed. The difference in observed radius is more likely if variation in tidal heat across Io affects crustal density rather than crustal thickness. Then, it is more likely that Io does not have a magma ocean.

1 Introduction

It is presently a mystery whether Jupiter's hyper-volcanic satellite, Io, hides a magma ocean beneath its lithosphere (e.g., de Kleer et al., 2019; Matusyama et al., 2022). Potential evidence for such a magma ocean includes a magnetic induction signal measured by the Galileo spacecraft mission; however, such a signal could also be indicative of a magmatic sponge layer that is a mix of rock and melt (Khurana et al., 2011). Moreover, the distribution of volcanoes on Io's surface may be indicative of a concentration of tidal dissipation in the shallow mantle (e.g., Tackley et al., 2001; Tyler et al., 2015). Miyazaki and Stevenson (2022) argue such a distribution could instead be the result of heterogeneities in lithospheric weakness, as the presence of a magma ocean may redistribute any spatial variations in tidal heating due to said magma ocean. Further, they argue that a partial-melt layer within Io's subsurface is inherently unstable and would instead separate into a solid and liquid phase (Miyazaki & Stevenson, 2022). The presence of a magma ocean within Io's subsurface would have implications for the distribution and transport of tidal heating within the satellite (e.g., Matusyama et al., 2022).

In recent work, Gyalay and Nimmo (2023) demonstrated how to use the observed long-wavelength topography of Saturn's icy satellites to infer the tidal heating distribution beneath their ice shells, which provides an indirect window into their interior structure. We first investigate if such a methodology may be applied to Io by assuming Io's degree-2 shape is a combination of its hydrostatic shape (due to Io's rotational flattening and tidal buldge) and topographic variations due to the spatial pattern of tidal heating. Upon subtraction of Io's hydrostatic shape, however, we find the remnant topography is lower than the uncertainty in Io's global shape (see Section S2 of Supplement 1). While we thus cannot meaningfully apply the methodology of Gyalay and Nimmo (2023a), the uncertainty nonetheless places a useful upper bound on the amplitude of topography that spatial variations tidal heating may produce. We use this constraint to make a prediction on the presence or absence of a magma ocean that may be confirmed by upcoming Juno flybys (Keane et al., 2022). In particular, we find that Airy isostasy produces topographic amplitudes that are too large, while Pratt isostasy does not. Since Airy isostasy is likely to dominate if a magma ocean is present, we conclude that Io probably lacks a magma ocean.

2 Background

The spatial variation of tidal heating across a satellite depends greatly on the depth or thickness of the tidal-heat-producing region (e.g., the crust, lithosphere, aesthenosphere, etc.), whether the tidal-heat-producing region overlies a more rigid (e.g., rocky mantle) or a more fluid (e.g., magma ocean) layer, and whether the tides are caused by the satellite's eccentricity (orbit's ellipticity) or obliquity (tilt of the satellite's spin axis relative to the normal of its orbital plane) (e.g., Segatz et al., 1988; Beuthe, 2013). In recent work, Gyalay and Nimmo (2023a) demonstrated the use of the observed long-wavelength topography of Saturn's icy satellites to infer the tidal heating distribution beneath their ice shells.

In principle, a similar methodology could be applied to Io's topography in order to test whether it was the result of spatial variations in tidal heating consistent with a magma ocean beneath Io's lithosphere.

Previous studies have investigated the link between Io's tidal heating and its lithospheric thickness (Steinke et al., 2020a; Spencer et al., 2021), where the lithospheric thickness can be related to topography under the assumption of isostasy (see the next section, Section 3). The average surface heat flow of Io is at least 2 W m^{-2} (Veeder et al., 1994; Simonelli et al., 2001; McEwen et al., 2004; Rathbun et al., 2004; de Kleer et al., 2019). This significant quantity of heat is generated frictionally by tidal stresses as a result of Io's Laplace resonance with Europa and Ganymede (predicted by Peale et al., 1979, mere weeks before Voyager 1's flyby). This tidal heating vastly dominates the surface heat flow, which would be only 0.016 W m^{-2} if Io's entire mass had the radioactive heat production rate of Earth's mantle (7.38 pW kg^{-1}, e.g., Turcotte & Schubert, 2014). As Io's core is not radioactive, even that value is an upper bound.

If tidal heat were simply conducted to the surface, the lithosphere would need to be less than a few km thick (e.g., O'Reilly & Davies, 1981). However, Io's surface is dotted with mountains that can reach heights > 10 km (e.g., Carr et al., 1979, 1998; Schenk et al., 2001). In Section S1 of Supplement 1, we estimate that this requires a minimum lithosphere thickness of 23 km (cf. values of 14-50 km in Nash et al., 1986; Keszthelyi & McEwen, 1997; Carr et al., 1998; Jaeger et al., 2003; McEwen et al., 2004). O'Reilly and Davies (1981) argued that to satisfy the seemingly-paradoxical, observed constraints of Io's mountainous terrain and high surface heat flux, Io must advect much of its heat through a thick, cold lithosphere via heat pipes of magma that erupt upon the surface. Spencer et al. (2021) incorporated this effect into their study by using melt production from tidal dissipation to heat the lithosphere and predict surface topography. Our approach differs from theirs in a few key ways, as elaborated upon below.

We make the simplifying assumption that if tidal heating operates at the base of the lithosphere or deeper, it provides a total surface heat flux F as described by Equations 1 and 3b of O'Reilly and Davies (1981):

$$F = v\rho \left[\Delta H_f + C_p \left(T_m - T_s\right)\right] + \frac{v\rho C_p \left(T_m - T_s\right)}{e^{vd/\kappa} - 1}, \tag{1}$$

where v is the resurfacing rate, ρ is the magma density, ΔH_f is the latent heat of fusion, C_p is the specific heat, T_m is the melting temperature, T_s is the surface temperature, κ

Table 1. Variables and their (Preferred) Values

	Variable	(Pref.) Value	Note
F	Surface heat flux	$F_0 > 2$ W m^{-2}	Observed[a]
d	Lithosphere thickness	$d_0 > 23$ km	Section S1 of Supplement 1
v	Volcanic emplacement rate	$v_0 > 10.7$ mm yr^{-1} $\left(v_0 > 0.34 \text{ nm s}^{-1}\right)$	Eq. 1 for $d = 23$ km, $F = 2$ W m^{-2}
ρ	Magma density	3,000 kg m^{-3}	O'Reilly and Davies (1981)
$\Delta\rho$	Density contrast	300 kg m^{-3}	
ΔH_f	Latent heat of fusion	450 kJ kg^{-1}	O'Reilly and Davies (1981)
C_p	Specific heat	1 kJ kg^{-1} K^{-1}	O'Reilly and Davies (1981)
T_s	Surface temperature	110 K	Rathbun et al. (2014)
T_m	Melting temperature	$T_m - T_s = 1,500$ K	O'Reilly and Davies (1981)
k	Thermal conductivity	3 W m^{-1} K^{-1}	O'Reilly and Davies (1981)
κ	Thermal diffusivity	10^{-6} m^2 s^{-1}	O'Reilly and Davies (1981)
α	Volumetric thermal expansivity	3×10^{-5} K^{-1}	
Q_A	Activation energy	300 kJ mol^{-1}	
R_G	Universal gas constant	8.3 J mol^{-1} K^{-1}	
R_0	Io radius	1,800 km	Observed
g	Surface gravity	1.8 m s^{-2}	Observed
C	Moment of Inertia	0.3782 M R_0^2	Schubert et al. (2004)

[a]Veeder et al. (1994); Simonelli et al. (2001); McEwen et al. (2004); Rathbun et al. (2004); de Kleer et al. (2019)

is the thermal diffusivity, and d the lithospheric thickness. One can also find the thermal conductivity of the lithosphere k as $k = \rho C_p \kappa$. Table 1 lists our preferred values for these variables, which borrow largely from O'Reilly and Davies (1981). The first term on the right-hand side of Equation 1 provides the portion of heat flux that is advected through heat pipes to the surface, while the second term provides the portion of heat flux that is conducted through the lithosphere. In the limit of low volcanic emplacement v, we recover Fourier's law of thermal conduction through a slab.

At a given lithospheric thickness, Equation 1 implies a larger volcanic emplacement rate produces a higher heat flux; while for a given resurfacing/emplacement rate, the lithosphere thins when tidal dissipation increases. The latter point can also be seen by inverting Equation 1 to solve for d,

$$d = \frac{\kappa}{v} \ln \left(\frac{v\rho C_p \left(T_m - T_s\right)}{F - v\rho \left[\Delta H_f + C_p \left(T_m - T_s\right)\right]} + 1 \right). \quad (2)$$

Equation 1 or 2 only satisfies both the minimum average surface heat flux $F > 2$ W m^{-2} and our minimum average lithosphere thickness $d > 23$ km for Io when the conductive heat flux is a small fraction of the total heat flux, $F_{cond} < 3 \times 10^{-4} F$. Alternatively, one may simply state that the total heat flux is dominated by the advective term, $F \sim F_{adv}$. This requires an average volcanic emplacement rate of $v = 10.7$ mm yr^{-1} (3.4×10^{-10} m s^{-1}) when $F = 2$ W m^{-2}.

By inferring the spatial distribution of tidal heating from topography, we may make inferences about the interior structure of Io. But first we must isolate the portion of Io's topography that arises from variations in tidal heating. Tidal heating varies spatially in even-orders of spherical harmonic degrees 2 and 4. We would thus wish to analyze Io's topography in those same spherical harmonics (e.g., Gyalay & Nimmo, 2023a). Unfortunately, we find in Section S2 of Supplement 1 that after accounting for the hydrostatic component of Io's shape (i.e., that which is due to Io's tidal bulge and rotational flattening), Io's remaining topography in those spherical harmonics is less than the uncertainty in global shape. Any conclusion on patterns of tidal heating inferred from this topography is then meaningless.

However, the *magnitude* of topographic variation may still yield some important constraints. In our case, the maximum (non-hydrostatic) topographic variation is limited by the uncertainty in degree-2 shape, which is on the order of 0.3 km (Section S2 of Supplement 1). In, e.g., Beuthe (2013), the heat flux due to tidal heating can vary spatially in magnitude on the order of its average value. Io would not be as hot as it is without significant tidal heating (Peale et al., 1979). Then it stands to reason that most (if not all) of Io's heat flow is due to tidal heating. Given some variation in tidal heating, we can calculate the expected variation in Io's topography and compare it to our bounds on the possible variation in Io's topography.

3 Predicting Isostatic variation in Io's topography

We make the assumption that Io's crust is in isostatic equilibrium at long wavelengths (low spherical harmonic degree). In any form of isostasy, we expect that either the total mass or pressure at some depth to be constant across a planetary body despite variations in the topography (see, e.g., Hemingway & Masuyama, 2017, for an argument in favor of equal-pressure isostasy). An alternate treatment of isostasy seeks to minimize the deviatoric stress within the crust (Beuthe, 2021). Minimum-stress isostasy can be approximated by equal-weight isostasy, which returns results between those of equal-mass and equal-pressure isostasy. In Gyalay and Nimmo (2023a), we used both equal-mass and equal-pressure isostasy as endmember cases in examining the ice shell of Tethys. Ultimately, interpretation of Tethys' interior was consistent across both treatments of isostasy. However, as we do not expect a significantly thick lithosphere on Io relative to its total radius, constant-pressure isostasy and constant-mass isostasy are nearly identical. Therefore in this paper, we default to the simpler calculations using equal-mass isostasy.

Beyond the choice of equal-mass, equal-pressure, equal-weight, or minimum-stress isostasy, there are still two overarching types of isostasy: Airy isostasy wherein topography is due to crustal thickness variations (more likely in the case of a magma ocean) or Pratt isostasy where topography is due to crustal density variations. In this manuscript, we apply these isostatic assumptions to the entire lithosphere (i.e., both the crust *and* the uppermost layer of the mantle) rather than just the crust. We assume that the bulk density of the crust plus uppermost mantle can differ from that of the mantle beneath, because of petrological differences arising during melt production and transport. The presence of heat pipes transporting melt from the mantle to the surface further necessitate another assumption: the dependence of volcanic emplacement rate v upon variations in heat flow F. We examine two endmember states: either v is a constant value $v = v_0$, or v varies in direct proportion to the local surface heat flux $v = v_0F/F_0$, where F_0 is the average heat flow. In comparison, Spencer et al. (2021)'s treatment of Pratt isostasy in Io's lithosphere makes the distinction between the abundance of heat pipes and the flux of melt through each heat pipe. They hold either the pipe density uniform (but allow flow to vary in each) or the flow through any pipe constant (but allow variation in the concentration of heat pipes). However, this extra flexibility requires the assumption of additional constants to relate the values to v. We avoid having to make such assumptions with our approach.

In the limit of strong tidal heating, the amplitude of heat flux variations δF in spherical harmonic degree-2 (where $\delta F = F - F_0$) approaches the average total heat flux F_0 (e.g. Beuthe, 2013). Then, we may test which of our cases predict isostatic topography as a function of spatial variations in tidal heating that is consistent with a maximum amplitude of ~ 0.3 km. We plot the expected topography as a function of heat flux variation for each mode of isostasy (Pratt or Airy) and dependence of emplacement rate on local heat flux ($v = v_0$ or $v \propto F$) in Figure 1.

3.1 Airy Isostasy

If there is a sub-surface magma ocean, we would expect Airy isostasy as with the floating shells of icy satellites. Here, we assume the topography is driven by variations in lithospheric thickness. To maintain a constant pressure at depth, lithospheric thinning would result in negative surface topography, and vice versa. We can relate topography h to a change in lithospheric thickness δd:

$$h = \frac{\delta d}{\left(1 + \frac{\rho}{\Delta\rho}\right)}, \tag{3}$$

where $\Delta\rho$ is the density contrast between the lithosphere and the underlying material. If the magma is sourced from the upper mantle and is denser than the lithosphere, a topographic high is the result of a thicker lithosphere. If instead the magma is sourced from the base of the crust and is less dense than the lithosphere (as a whole), then this equation implies a topographic high is the result of a thinner lithopshere. However, that latter scenario is inherently unstable and subject to overturn of the lithosphere. We therefore assume the lithosphere is 300 kg m^{-3} less dense than the magma.

3.1.1 Constant v case

If we assume the emplacement rate v is uniform across Io's surface in the case of Airy isostasy, we can begin with Equation 2 to calculate the expected topography h for some given variation in heat flux δF from the mean F_0. After setting $v = v_0$, the difference in lithospheric thickness δd calculated by subtracting the mean d_0 from Equation 2 is,

$$\delta d = \frac{\kappa}{v_0} \ln\left(\frac{v_0 \rho C_p \left(T_m - T_s\right)}{F_0 + \delta F - v_0 \rho \left[\Delta H_f + C_p \left(T_m - T_s\right)\right]} + 1\right) - d_0. \tag{4}$$

Note that $v_0 \rho \left[\Delta H_f + C_p \left(T_m - T_s\right)\right]$ is the advective heat flux, F_{adv}. Then,

$$\delta d = \frac{\kappa}{v_0} \ln\left(\frac{v_0 \rho C_p \left(T_m - T_s\right) \frac{1}{F_0}}{1 + \frac{\delta F}{F_0} - \frac{F_{adv}}{F_0}} + 1\right) - d_0. \tag{5}$$

Then because the conductive heat flux $F_{cond} = v \rho C_p \left(T_m - T_s\right) / \left(e^{vd/\kappa} - 1\right)$, we may further rearrange the equation and substitute δd into Equation 3 to find,

$$h = \frac{1}{1 + \frac{\rho}{\Delta\rho}} \left[\frac{\kappa}{v_0} \ln\left(\frac{\frac{F_{cond,0}}{F_0} e^{v_0 d_0/\kappa} + \frac{\delta F}{F_0}}{\frac{F_{cond,0}}{F_0} + \frac{\delta F}{F_0}}\right) - d_0\right], \tag{6}$$

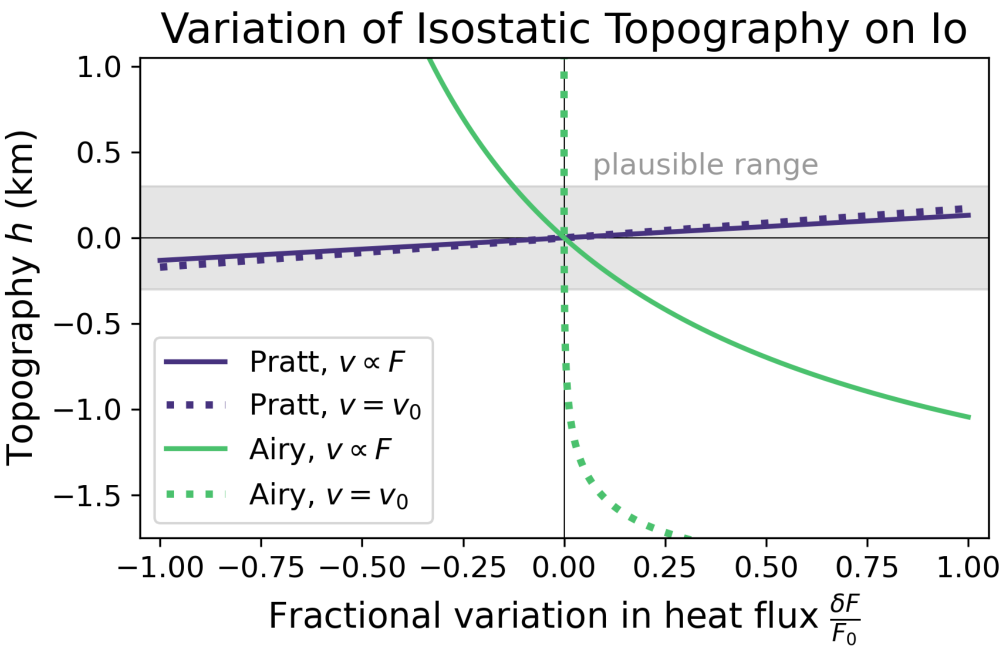

Figure 1. We plot the variation of Io's isostatic long wavelength topography as a function of heat flux, as compared to the amplitude of topography $|h| < 0.3$ km allowed by the uncertainty in Io's global shape (gray region). Topography that assumes Airy isostasy and $v = v_0$ (dotted green line) is characterized by Equation 6 for $F_{cond,0} = 2.95 \times 10^{-4} F_0$, which is the maximum value allowed for the minimum average lithospheric thickness $d_0 = 23$ km and minimum average heat flux $F_0 = 2$ W m^{-2}. Increasing d_0 would further limit $F_{cond,0}$ and the maximum variability of δF. Topography that assumes Airy isostasy and $v \propto F$ (solid green line) is characterized by Equation 8 for minimum average lithospheric thickness $d_0 = 23$ km. Larger d_0 would increase topography as a function of heat flux variation. Topography that assumes Pratt isostasy and $v = v_0$ (dotted purple line) is characterized by Equation 21 for minimum average volvanic emplacement $v_0 = 10.7$ mm yr^{-1}. Topography that assumes Pratt isostasy and $v \propto F$ is characterized by Equation 28 for the same assumed v_0. Larger v_0 would reduce variation in h for both cases of Pratt isostasy. All other parameters use the preferred values in Table 1.

where $F_{cond,0}$ is F_{cond} at $d = d_0$ and $v = v_0$. Because F_{adv} remains constant if $v = v_0$, then $|\delta F| < F_{cond,0}$, where $F_{cond,0} < 3\times10^{-4}$ for the preferred value of our parameters in Table 1. Further, in Equation 6 we can easily see that the topography is undefined if $\delta F = -F_{cond,0}$. Thus, it is impossible for tidal heat flux variations on the order of the average heat flux $|\delta F| \sim F_0$ to exist for an Io lithosphere under Airy isostasy with constant emplacement rate v_0 unless the total heat flux were dominated by the conductive term.

3.1.2 $v \propto F$ case

When v is instead proportional to F in the case of Airy isostasy, we substitute $v = v_0 F/F_0$ into Equation 1 and solve for F:

$$F = \frac{F_0}{d}\frac{\kappa}{v_0}\ln\left(\frac{v_0\rho C_p(T_m - T_s)}{F_0 - v_0\rho[\Delta H_f + C_p(T_m - T_s)]} + 1\right). \tag{7}$$

When compared to Equation 2, we may simplify Equation 7 to $Fd = F_0 d_0$. Substituting $d = d_0 + \delta d$ and Equation 3 into Equation 7, we rearrange and find

$$h = \frac{-d_0}{\left(1 + \frac{\rho}{\Delta\rho}\right)}\frac{\frac{\delta F}{F_0}}{\left(1 + \frac{\delta F}{F_0}\right)}. \tag{8}$$

When $|\delta F| \sim F_0$ we should expect the amplitude of topography h in degree-2 to reach about $d_0/20$. If $h \leq 0.3$ km, then this is only true when $d_0 \leq 6$ km—which is thinner than the $\sim$ 23 km minimum average thickness we expect for Io's lithosphere (Section S1 of Supplement 1).

3.2 Pratt Isostasy

Under Pratt isostasy, we expect topography to be the result of density variations in the lithosphere. Traditionally, Pratt isostasy also assumes the base of the lithosphere is "flat" and there is no basal topography. For Io, this is less certain (cf., Spencer et al., 2021), but as a combination of Pratt and Airy would be dominated by the effects of Airy isostasy, we assume this traditionally flat basal topography as an endmember case. To maintain constant pressure at depth, density variations in the lithosphere $\delta\rho$ from a reference average lithospheric density ρ_0 are

$$\delta\rho = -\rho_0\frac{h}{d_0}. \tag{9}$$

Assuming density variations are due only to thermal expansion or contraction of the lithosphere, we relate the change in crustal density to the change in the lithosphere's average temperature $\delta\bar{T}$ from some reference temperature $\bar{T}_0$ for a thermal expansivity α:

$$\delta\bar{T} = -\frac{\delta\rho}{\alpha\rho_0} = \frac{\delta d}{\alpha d_0} = \frac{h}{\alpha d_0}, \tag{10}$$

where the final equality makes use of the fact that $\delta d = h$ in Pratt isostasy. It then behooves us to calculate the average temperature of the lithosphere and relate it to the heat flux through the lithosphere. O'Reilly and Davies (1981) provide the temperature profile as a function of depth z (where $z = 0$ is the surface, and $z = d$ is the base of the lithosphere):

$$T(z) = T_s + (T_m - T_s)\frac{e^{vz/\kappa} - 1}{e^{vd/\kappa} - 1}. \tag{11}$$

By taking the integral of Equation 11, we can find the average temperature of the lithosphere:

$$\bar{T} = \frac{1}{d}\int_0^d T(z)\,dz, \tag{12}$$

Finding

$$\bar{T} = T_s + (T_m - T_s)\Big(\frac{\kappa}{vd} - \frac{1}{e^{vd/\kappa} - 1}\Big), \tag{13}$$

which agrees that for high emplacement rates or thick lithospheres, most heat transport is accomplished by the advection of magma and thus the lithosphere's average temperature will be closer to the the surface temperature than the melting temperature. If v or d approaches 0, we can take the approximation $e^{vd/\kappa} \approx 1 + \frac{vd}{\kappa} + \frac{1}{2}(\frac{vd}{\kappa})^2$ and we find that $\bar{T}$ approaches $(T_m - T_s)/2$, which is what we expect in the case without heat pipes. Spencer et al. (2021) also assume Pratt isostasy in Io's lithosphere would be dominated by thermal expansion.

In our study, we explicitly vary the volcanic emplacement rate v and lithospheric thickness d, but hold the surface temperature T_s constant. T_m can vary in some unknown manner, so in our formalism for translating the topography δd into heat flux F via Pratt isostasy, we want to eliminate the dependence of T_m before we continue our derivation. We can rearrange Equation 13 to find

$$T_m - T_s = \frac{\bar{T} - T_s}{\frac{\kappa}{vd} - \frac{1}{e^{vd/\kappa} - 1}}. \tag{14}$$

Substituting Equation 14 into Equation 1 and rearranging, we find

$$F = v\rho\left[\Delta H_f + \frac{vd}{\kappa}(\bar{T} - T_s)\frac{e^{vd/\kappa}}{e^{vd/\kappa} - 1 - \frac{vd}{\kappa}}\right]. \tag{15}$$

For our minimum values of v, d, and F (Table 1), vd/κ is at minimum 7.8; implying $e^{vd/\kappa} > 2400$. Then, the fraction $e^{vd/\kappa}/\left(e^{vd/\kappa} - 1 - \frac{vd}{\kappa}\right)$ is only greater than unity by a maximum of 0.4%, meaning we may safely neglect the fraction for our consideration of Pratt isostasy. Simpler now, we find,

$$F \approx v\rho \left[\Delta H_f + \frac{vd}{\kappa} C_p(\bar{T} - T_s) \right]. \tag{16}$$

3.2.1 Constant v case

If we assume emplacement rate v is uniform across Io's surface in the case of Pratt isostasy, we can substitute $v = v_0$ into Equation 16. Then, one would expect the difference in heat flux from average δF to be

$$\delta F \approx \frac{v_0^2 \rho C_p}{\kappa} [d_0 \delta \bar{T} + h(\bar{T}_0 - T_s) + h\delta \bar{T}]. \tag{17}$$

When we substitute $\delta \bar{T} = h/(\alpha d_0)$ (Equation 10) into Equation 17, we find the variation in heat flux through Io's lithosphere under Pratt isostasy and constant volcanic emplacement $v = v_0$ as,

$$\delta F \approx \frac{v_0^2 h \rho C_p}{\kappa} \left[\frac{1}{\alpha} \left(1 + \frac{h}{d_0} \right) + \left(\bar{T}_0 - T_s \right) \right]. \tag{18}$$

In the first term within the square brackets, we expect $\frac{h}{d_0} \ll 1$, meaning we can drop the second term within those parentheses for this approximation. A reasonable volumetric thermal expansivity for rock at $\bar{T}$ is $\alpha \sim 3 \times 10^{-5}$ K^{-1}, meaning that $\bar{T}_0 - T_s \ll \alpha^{-1}$, and we may drop that second term. Thus, our relationship between topography h and variation in tidal heating δF can be reduced to,

$$\delta F \simeq \frac{v_0^2 \rho C_p}{\kappa \alpha} h. \tag{19}$$

Keeping in mind that $F_0 \sim F_{adv}$, we can account for variations in F as a factor of itself by dividing both sides of Equation 19 by F_0 or F_{adv},

$$\frac{\delta F}{F_0} \sim h \frac{v_0}{\kappa} \frac{C_p \frac{1}{\alpha}}{\Delta H_f + C_p (T_m - T_s)}. \tag{20}$$

Solving now for the topography h,

$$h \sim \frac{\delta F}{F_0} \frac{\kappa}{v_0} \alpha \left[\frac{\Delta H_f}{C_p} + (T_m - T_s) \right]. \tag{21}$$

If heat flux varies on the order of itself ($|\delta F| \sim F_0$), then we expect the amplitude of h to reach about $h \sim 172$ m $\times \frac{\delta F}{F_0} \frac{10.7 \text{ mm yr}^{-1}}{v_0}$ (where $v_0 = 10.7$ mm yr^{-1} is the minimum average volcanic emplacement expected for the minimum observed average heat flux of

$F \sim 2$ W m^{-2}), which would create long-wavelength topography *less* than the maximum possible degree-2 topography (as limited by our uncertainty, Section S2 of Supplement 1).

3.2.2 $v \propto F$ case

When v is instead proportional to F in the case of Pratt isostasy, we substitute $v = v_0 F/F_0$ into Equation 16 and rearrange to find

$$\frac{F}{F_0} \approx \frac{F_0 - v_0 \rho \Delta H_f}{\frac{v_0 d}{\kappa} v_0 \rho C_p \left(\bar{T} - T_s\right)}. \tag{22}$$

In this case, the variation in F is due to variation in the $1/[d(\bar{T} - T_s)]$ term. Neither d nor $\bar{T}$ are expected to vary greatly, and thus we make the approximation

$$\delta \left[\frac{1}{d\left(\bar{T} - T_s\right)}\right] \simeq -\frac{\left[d_0 \delta \bar{T} + h\left(\bar{T}_0 - T_s\right)\right]}{d_0^2 (\bar{T}_0 - T_s)^2}. \tag{23}$$

Thus,

$$\frac{\delta F}{F_0} \simeq -\frac{\left(F_0 - v_0 \rho \Delta H_f\right)\left[d_0 \delta \bar{T} + \delta d\left(\bar{T}_0 - T_s\right)\right]}{v_0^2 d_0^2 k \left(\bar{T}_0 - T_s\right)^2}. \tag{24}$$

When we substitute $\delta \bar{T} = h/\left(\alpha d_0\right)$ (Equation 10) into Equation 24, we find the variation in heat flux through Io's lithosphere under Pratt isostasy and volcanic emplacement rate proportional to heat flux variations $v = v_0 F/F_0$ as,

$$\frac{\delta F}{F_0} \simeq -\frac{\left(F_0 - v_0 \rho \Delta H_f\right)\left[\frac{1}{\alpha} + \left(\bar{T}_0 - T_s\right)\right] h}{v_0^2 d_0^2 k \left(\bar{T}_0 - T_s\right)^2}. \tag{25}$$

Then, using Equation 14, the $\bar{T}_0 - T_s$ term within the square brackets can be substituted with $\bar{T}_0 - T_s = (T_{m,0} - T_s)\left[\frac{\kappa}{vd} - \frac{1}{\exp\left(vd/\kappa\right) - 1}\right]$. Assuming $T_m - T_s = 1{,}500$ K, this term is a *maximum* of 193 K (for our minimum v_0 and d). Meanwhile, α^{-1} is *always* much greater than $\left(\bar{T}_0 - T_s\right)$. Thus, our relationship between topography and variation in tidal heating δF can be reduced to,

$$\frac{\delta F}{F} \sim \frac{F_0 - v_0 \rho \Delta H_f}{\frac{v_0 d_0}{\kappa} v_0 \rho C_p \left(\bar{T}_0 - T_s\right)} \times \frac{-1}{\alpha\left(\bar{T}_0 - T_s\right)} \frac{h}{d_0}. \tag{26}$$

If one substitutes $\bar{T}_0 - T_s$ with Equation 10, they will find the denominator of the first fraction in Equation 26 will very nearly be equivalent to $F_0 - v_0 \rho \Delta H_f$ (Equation 1) and thus reduce the fraction to 1. Then,

$$\frac{\delta F}{F_0} \sim -\frac{v_0}{\kappa} \frac{h}{\alpha\left(T_{m,0} - T_s\right)}. \tag{27}$$

Finally, rearranging to solve for h,

$$h \sim \frac{\delta F}{F_0} \frac{\kappa}{v_0} \alpha \left(T_m - T_s\right). \tag{28}$$

If heat flux varies on the order of itself ($|\delta F| \sim F_0$), then we expect the amplitude of h to reach about $h \sim 132\ \mathrm{m} \times \frac{\delta F}{F_0} \frac{10.7\ \mathrm{mm\ yr^{-1}}}{v_0}$.

4 Implications and Discussion

Should Io have a magma ocean, we might expect its lithosphere to experience Airy isostasy rather than Pratt isostasy. However, when assuming Airy isotasy, we find in both the constant $v = v_0$ and proportional $v \propto F$ cases of volcanic emplacement that the resulting degree-2 topography is far greater than the maximum possible topography as limited by our uncertainty (Figure 1). Thus, it is impossible for Io lithosphere's lithosphere to be in Airy isostasy if the variation in heat flux is as great as one would expect from tidal heating. Instead, this would imply that the heat flux is a mostly uniform background. Io cannot generate this much heat radioactively, so if Io were in Airy isostasy, some additional process would need either to erase either Io's topography in response to strong tidal heat variations *or* any spatial variation in the tidal heat that would produce this topography.

However, it *is* possible for Io to produce its expected long-wavelength topography while under strong tidal heating variations on the order of its average tidal heat flux—*if* Io's lithosphere operates under Pratt isostasy. This is true both when volcanic emplacement rate is uniform across Io's surface and when variation in volcanic emplacement rate is proportional to variations in tidal heating (Figure 1). In both cases, we expect the amplitude of degree-2 topography to reach about ~ 150 m when average volcanic emplacement rate v is that which is expected for the observed minimum average heat flow (Table 1).

Before eliminating the possibility of Airy isostasy, we explore the reasons why there may not be significant topography in response to expected variations of tidal heating.

4.1 Topographic relaxation

One reason why Io might not have significant topography if it were in Airy isostasy could be lower crustal (here, lithospheric) flow. The warmest portion of the lithosphere will tend to have the lowest viscosity and will flow laterally in response to horizontal pressure gradients (e.g., McKenzie et al., 2000; Nimmo & Stevenson, 2001; Nimmo, 2004). That is, the deepest roots of the lithosphere will naturally want to smooth out and reduce its basal topography. Typically, this timescale is much longer than that for attaining isostatic topography in the first place (e.g., Nimmo & Stevenson, 2001). We examine here if this holds true for Io as well.

As for the crusts of many planetary bodies, the dynamic viscosity η of Io's lithosphere is expected to vary exponentially with its temperature, $\eta \propto \exp\left[Q_A/\left(R_G T\right)\right]$, where Q_A is the activation energy of the rock that makes up the lithosphere and R_G is the universal gas constant. Because the viscosity depends exponentially upon the temperature within the lithosphere, we expect only the base of Io's lithosphere to have a viscosity low enough to flow laterally. The thickness of this flowing region is a few times some characteristic lengthscale δ_{flow}. Then, the timescale τ_{rel} to relax (reduce) the amplitude of sinusoidal variations in topography in spherical harmonic degree l by a factor of e is provided by Nimmo (2004) as

$$\tau_{rel} = \frac{\eta_0}{\Delta\rho g}\left(\frac{R_0}{l}\right)^2 \frac{1}{\delta_{flow}^3}, \tag{29}$$

where η_0 is the reference viscosity at the base of the lithosphere (where $T = T_m$), and R_0 is Io's average radius (listed in Table 1). We focus on spherical harmonic degree $l = 2$, where the greatest variation in tidal heating is expected. At $l = 2$, the wavelength of topographic variation is half of Io's circumference.

As one might expect from a lengthscale that characterizes the thickness of the flowing region of a lithosphere when its viscosity depends exponentially on temperature, δ_{flow} depends on the vertical temperature gradient $\frac{\partial T}{\partial z}$ at the base of the lithosphere, where z is depth measured from Io's surface. Following Nimmo and Stevenson (2001), if viscosity depends on temperature as $\eta \sim e^{Q_A/(R_G T)}$ and the temperature gradient at some distance $\Delta z = d - z$ above the base of the lithosphere (thickness d) is approximately linear, then

$$\exp\left(\frac{Q_A}{R_G T}\right) \approx \exp\left(\frac{Q_A}{R_G T_m}\right) \exp\left(\frac{\Delta z}{\delta_{flow}}\right). \tag{30}$$

Thus,

$$\delta_{flow} \simeq \frac{R_G}{Q_A} \frac{T_m^2}{\left.\frac{\partial T}{\partial z}\right|_{z=d}} \tag{31}$$

(cf., Nimmo & Stevenson, 2001; Nimmo, 2004).

Were Io's lithosphere to be in a purely conductive regime (very thin crust), we would find $\delta_{flow} = R_G k T_m^2/\left(Q_A F_{cond}\right)$. However, because we expect Io to have a lithospheric thickness $d > 23$ km (Section S1 of Supplement 1), we must instead take the derivative of Equation 11 to find

$$\delta_{flow} = \frac{R_G}{Q_A}\frac{\kappa}{v}\frac{T_m^2}{(T_m - T_s)}. \tag{32}$$

This is substantially smaller than what one expects in a purely conductive regime, by a factor of about $3F_{adv}/(4F_{cond})$. This is because the temperature profile we expect in Io's lithosphere (Equation 11) is relatively close to the surface temperature T_s until $z \to d$ and the temperature exponentially climbs to T_m. Assuming Io's lithosphere has an activation energy of ~ 300 kJ mol^{-1}, δ_{flow} is only about 100 m.

Such a low δ_{flow} vastly increases the amount of time it would take to relax Io's isostatic topography. Meanwhile, the timescale to attain topography in isostatic equilibrium τ_{iso} is $\tau_{iso} \sim \eta_M l/(2\pi\rho_M g R_0)$ (Nimmo & Stevenson, 2001), where η_M is mantle viscosity and ρ_M is mantle density. Then, a comparison of the two timescales yields

$$\frac{\tau_{rel}}{\tau_{iso}} = 2\pi\frac{\eta_0}{\eta_M}\frac{\rho_M}{\Delta\rho}\left(\frac{R_0}{\delta_{flow} l}\right)^3, \tag{33}$$

where with our preferred values (Table 1) is about $10^{14}\ \eta_0/\eta_M$. This means that for lower crustal flow to reasonably erase any long-wavelength topography due to variations in tidal heating, Io's mantle would need to be 10^{11} times more viscous than the base of its lithosphere. While the viscosity profile of Io is poorly constrained (cf., Lainey et al., 2009; Bierson & Nimmo, 2016; Steinke et al., 2020a, 2020b; Spencer et al., 2021), such a contrast sparks incredulity. Thus, it is unlikely that in the event of Airy isostasy, topography would be subdued by lower lithospheric flow.

4.2 Tidal heat redistribution

Another possibility to investigate is the redistribution of tidal heat flux into a more uniform heating pattern. Assuming the case where volcanic emplacement rate $v \propto F$, we may rearrange Equation 8 to find

$$\frac{|\delta F|}{F_0} = \frac{1}{1 + \frac{d_0}{h\left(1+\frac{\rho}{\Delta\rho}\right)}}. \tag{34}$$

For maximum degree-2 topography of $h \sim 0.3$ km (Section S2 of Supplement 1) and minimum lithosphere thickness of $d_0 \sim 23$ km (Section S1 of Supplement 1), we find that variations in heat flux must have a maximum $|\frac{\delta F}{F_0}| < 0.17$ to not violate the observed topography (see also Figure 1). By examining the volcano distribution, Steinke et al. (2020b) find that the magnitude of degree-2 coefficients of volcano density vary from

0.02 to 0.146× the average volcano density, which is consistent with our finding that degree-2 variations in heat flux are below 0.17 of the average. Hamilton et al. (2013) likewise argue that if Io's volcano distribution is related to a tidal heat distribution, then that heating pattern is approximately 20% tidal heating in Io's aesthenosphere with the rest either a uniform heat distribution or deep mantle heating. As less than 1% of Io's total heat production is radiogenic, then a uniform heat distribution would need to have been a tidal heating pattern that was blurred into appearing uniform.

The observed variation in surface heat flux δF_O may be related to the originally produced heat flux δF_P by some blurring function $B(l)$ that depends on the spherical harmonic degree l (e.g., Steinke et al., 2020a, 2020b). This assumes that there exists a convective layer beneath the lithosphere (typically the asesthenosphere) that produces its own heat tidally. Following Tackley (2001); Steinke et al. (2020a, 2020b), we find this blurring function to be

$$B\left(l\right) = \frac{R_0 \pi}{l d_{conv}} C_B \mathrm{Ra}_H^{-\beta}, \tag{35}$$

where d_{conv} is the thickness of the convecting layer, C_B and β are constants related to the blurring of the heat flux variations, and Ra_H is the Rayleigh-Roberts number (sometimes referred to as the internal-heating Rayleigh number), which characterizes the convective transport of heat-producing material as compared to the diffusion of its heat and is defined as

$$\mathrm{Ra}_H = \frac{\rho g \alpha H d_{conv}^5}{k \eta_{conv} \kappa}, \tag{36}$$

where H is the thermal productivity in the mantle in units of power per mass and η_{conv} is the dynamic viscosity of the convecting layer. Following Steinke et al. (2020a, 2020b), we approximate $H = f_{cc} F_P / d_{conv}$, where f_{cc} is the fraction of tidal heating produced in the convective layer F_P that is transported through the mantle by conduction and convection (as opposed to bouyant magmatism through the mantle).

In order for the spatial distribution of volcano density to resemble a tidal heating pattern whose heat flux varies approximately $\leq 17\%$ of the average heat flow, then $B(2) \leq 0.17$. That is,

$$\mathrm{Ra}_H \geq \left(\frac{R_0}{d_{conv}} \frac{\pi}{2} \frac{C_B}{0.17} \right)^{1/\beta}. \tag{37}$$

When heating is uniform within the convective layer, $C_B = 4.413$ and $\beta = 0.2448$, while when the heating is focused at the boundary of the layer, $C_B = 2.869$ and $\beta = 0.2105$ (Tackley, 2001). Depending on the regime then, this would mean Ra_H has to be greater than about 10^{13} to 10^{14} (assuming a convective layer thickness of 50 km) to reduce degree-2 tidal heating variations to 17%.

For constants in Table 1, we find this implies for such blurring to occur,

$$\frac{\eta_{conv}}{f_{cc}} \leq 7 \times 10^{10} \text{ Pa s} \left(\frac{F_P}{2 \text{ W m}^{-2}}\right) \left(\frac{d_{conv}}{50 \text{ km}}\right)^{4+\frac{1}{\beta}}. \tag{38}$$

Steinke et al. (2020b) find that f_{cc} is likely < 0.2. This then requires that if there were a circulating layer, its viscosity would be $< 10^{10}$ Pa s, which is lower than most estimates of asthenospheric viscosity (cf., Tackley, 2001; Steinke et al., 2020b). To achieve such a low viscosity might require the convecting layer to be a magma ocean—but then the amount of tidal heating produced within the convecting layer F_P would be greatly diminished. Furthermore, any heat produced by a magma ocean tides (e.g. Tyler et al., 2015) would be mainly due to the friction of the magma ocean dragging against the overlying lithosphere (cf. for ocean tides within icy satellites, Chen et al., 2014; Hay & Matsuyama, 2019).

The extent to which a magma ocean may instead redistribute a tidal heating pattern generated from *beneath* it rather than within it is presently unclear. However, we may draw an analogy with Europa, where it has been found that when ocean circulation has a weak dependence on rotation, such circulation has minimal effect upon the dispersion of tidal heating distributions from beneath (Soderlund et al., 2023). Thermal circulation in a potential magma ocean within Io would have an even weaker dependence on rotation, owing to the much higher viscosity of magma compared to water (a deeper discussion on how to characterize heat transfer in the circulating oceans of icy satellites may be found in Soderlund, 2019). Thus, we find it unlikely that a tidal heating pattern is redistributed by a convecting layer—whether the tidal heat is produced within a convecting aesthenosphere or produced beneath a convecting magma ocean.

5 Conclusions

Ultimately, we find that the maximum amplitude of isostatic topography that results from spatial variations in tidal heating across Io is irreconcilable with the expected spatial variation in tidal heating if we assume that Io's lithosphere operates under Airy isostasy. The amplitude of tidal heating variation in spherical harmonic degree 2 is expected to be on the order of average tidal heating. Instead, the assumption of Airy isostasy requires an amplitude of tidal heating variation $< 17\%$ of the average heat flow. A convective layer can produce and redistribute tidal heating into a relatively uniform heating pattern, but requires that this convective layer both produces most of Io's tidal heat *and* that this layer have an extremely low viscosity $< 10^{10}$ Pa s. An aesthenosphere could produce adequate internal tidal heating (i.e., not from drag at the base of the lithosphere) while a magma ocean may have a low enough viscosity, but neither possibility fulfills both conditions.

If we instead assume that Io's lithosphere operates under Pratt isostasy, then the predicted isostatic topography is consistent with the maximum allowed by the observations. Because we rule out Airy isostasy in favor of Pratt isostasy, this implies that a magma ocean is unlikely. This can soon be tested, as Juno's upcoming orbits of Jupiter will bring it close to Io. Already, recent infrared imagery has been used to analyze the distribution of Io's volcanic heat flow. Pettine et al. (2023) find that the tidal heating pattern implied by Io's volcano distribution is anti-correlated with a global magma ocean and instead suggests tidal heating in the aesthenosphere (cf., Davies et al., 2023), demonstrating a similar conclusion to our own using an entirely different dataset and method. Upcoming Juno flybys also allow the measurement of new gravitational data (Keane et al., 2022) that supplements measurements from older spacecraft. Such gravity observations could unveil Io's Love number k_2, which characterizes Io's tidal response. A high value of $k_2 \sim 0.5$ is expected if Io has a magma ocean, while a lower value $k_2 \sim 0.1$ is expected without a magma ocean (Bierson & Nimmo, 2016; de Kleer et al., 2019). Thus, we predict that if k_2 is measured for Io with Juno data, it will be low.

Open Research Section

This paper is purely theoretical, only deriving equations to apply to previously observed physical parameters. As such, no datasets were analyzed or produced for this paper. The python code used to create Figure 1 has been uploaded to the Dryad Repository and is listed in our References as Gyalay and Nimmo (2023b).

Acknowledgments

FN received funding from NASA Grant 80NSSC21K1802.

References

Beuthe, M. (2013). Spatial patterns of tidal heating. *Icarus*, *223*(1), 308–329. doi: 10.1016/j.icarus.2012.11.020

Beuthe, M. (2021). Isostasy with Love – i: elastic equilibrium. *Geophysical Journal*

International, *225*(3), 2157–2193. doi: 10.1093/gji/ggab073

Bierson, C. J., & Nimmo, F. (2016). A test for Io's magma ocean: modeling tidal dissipation with a partially molten mantle. *Journal of Geophysical Research: Planets*, *121*(11), 2211–2224. doi: 10.1002/2016JE005005

Carr, M. H., Masursky, H., Strom, R. G., & Terrile, R. J. (1979). Volcanic features of Io. *Nature*, *280*(5725), 729–733. doi: 10.1038/280729a0

Carr, M. H., McEwen, A. S., Howard, K. A., Chuang, F. C., Thomas, P., Schuster, P., ... Galileo Imaging Team (1998). Mountains and calderas on Io: Possible implications for lithosphere structure and magma generation. *Icarus*, *135*(1), 146–165. doi: 10.1006/icar.1998.5979

Chen, E. M. A., Nimmo, F., & Glatzmaier, G. A. (2014). Tidal heating in icy satellite oceans. *Icarus*, *229*, 11–30. doi: 10.1016/j.icarus.2013.10.024

Davies, A. G., Perry, J., Williams, D. A., & Nelson, D. M. (2023). *Io's polar volcanic thermal emission indicative of magma ocean and shallow tidal heating models.* (Preprint on Arxiv, `https://doi.org/10.48550/arXiv.2310.12382`) doi: 10.48550/arXiv.2310.12382

de Kleer, K., McEwen, A. S., Park, R. S., Bierson, C. J., Davies, A. G., DellaGiustina, D. N., ... Schneider, N. M. (2019). *Tidal heating: Lessons from Io and the Jovian system.* Final Report for the Keck Institute for Space Studies.

Gyalay, S., & Nimmo, F. (2023a). Estimates for Tethys' moment of inertia, heat flux distribution, and interior structure from its long-wavelength topography. *Journal of Geophsyical Research: Planets*, *128*(2). doi: 10.1029/2022JE007550

Gyalay, S., & Nimmo, F. (2023b). *Isostatic response of io's topography to the spatial variation of its tidal heating.* Dataset. Dryad. Retrieved from `https://datadryad.org/stash/share/YOzgrXbQG_GixJeSwZfZU98JdovcqvV1yJYAZGPZLhw` (This is a private URL for peer review. The repository will be made public with a doi for the final draft.)

Hamilton, C. W., Beggan, C. D., Still, S., Beuthe, M., Lopes, R. M. C., Williams, D. A., ... Wright, W. (2013). Spatial distribution of volcanoes on Io: Implications for tidal heating and magma ascent. *Earth and Planetary Science Letters*, *361*, 272–286. doi: 10.1016/j.epsl.2012.10.032

Hay, H., & Matsuyama, I. (2019). Nonlinear tidal dissipation in the subsurface oceans of Enceladus and other icy satellites. *Icarus*, *319*, 68–85. doi: 10.1016/j.icarus.2018.09.019

Hemingway, D., & Masuyama, I. (2017). Isostatic equilibrium in spherical coordinates and implications for crustal thickness on the Moon, Mars, Enceladus, and elsewhere. *Geophysical Research Letters*, *44*(15), 7695–7705. doi: 10.1002/2017GL073334

Jaeger, W. L., Turtle, E. P., Keszthelyi, L. P., Radebaugh, J., McEwen, A. S., & Pappalardo, R. T. (2003). Orogenic tectonism on Io. *Journal of Geophysical Research: Planets*, *108*(E8). doi: 10.1029/2002JE001946

Keane, J. T., de Kleer, K., & Spencer, J. (2022). Perspective: the future exploration of Io. *Elements*, *18*(6), 399–404. doi: 10.2138/gselements.18.6.399

Keszthelyi, L., & McEwen, A. (1997). Magmatic differentiation of Io. *Icarus*, *130*(2), 437–448. doi: 10.1006/icar.1997.5837

Khurana, K. K., Jia, X., Kivelson, M. G., Nimmo, F., Schuber, G., & Russell, C. T. (2011). Evidence of a global magma ocean in Io's interior. *Science*, *332*(6034), 1186–1189. doi: 10.1126/science.1201425

Lainey, V., Arlot, J., Karatekin, O., & Van Hoolst, T. (2009). Strong tidal dissipation in Io and Jupiter from astrometric observations. *Nature*, *459*, 957–959. doi: 10.1038/nature08108

Matusyama, I. N., Steinke, T., & Nimmo, F. (2022). Tidal heating in Io. *Elements*, *18*(6), 374–378. doi: 10.2138/gselements.18.6.374

McEwen, A. S., Keszthelyi, L. P., Lopes, R., Schenk, P. M., & Spencer, J. R. (2004). Jupiter: The planet, satellites and magnetosphere. In F. Bagenal, T. E. Dowling, & W. B. McKinnon (Eds.), (pp. 307–328). Cambridge University Press.

McKenzie, D., Nimmo, F., Jackson, J. A., Gans, P. B., & Miller, E. L. (2000). Characteristics and consequences of flow in the lower crust. *Journal of Geophysical Research: Solid Earth*, *105*, 11029–11046. doi: 10.1029/1999JB900446

Miyazaki, Y., & Stevenson, D. J. (2022). a subsurface magma ocean on Io: exploring the steady state of partially molten planetary bodies. *Planetary Science Journal*, *3*(11), 256. doi: 10.3847/PSJ/ac9cd1

Nash, D., Yoder, C., Carr, M., Gradie, J., & Hunten, D. (1986). Satellites. In J. A. Burns & M. S. Matthews (Eds.), (chap. Io: history of studies and current level of understanding of this satellite). University of Arizona Press.

Nimmo, F. (2004). Non-Newtonian topographic relaxation on Europa. *Icarus*, *168*(1), 205–208. doi: 10.1016/j.icarus.2003.11.022

Nimmo, F., & Stevenson, D. J. (2001). Estimates of Martian crustal thickness from viscous relaxation of topography. *Journal of Geophysical Research: Planets*, *106*(E3), 5085–5098. doi: 10.1029/2000JE001331

O'Reilly, T. C., & Davies, G. F. (1981). Magma transport of heat on Io: A mechanism allowing a thick lithosphere. *Geophysical Research Letters*, *8*(4), 313–316. doi: 10.1029/GL008i004p00313

Peale, S. J., Cassen, P., & Reynolds, R. T. (1979). Melting of Io by tidal dissipation. *Science*, *203*(4383), 892–894. doi: 10.1126/science.203.4383.892

Pettine, M., Imbeah, S., Rathbun, J., Hayes, A., Lopes-Gautier, R., Mura, A., ... Bertolino, S. (2023). *JIRAM observations of volcanic flux on Io: Distribution and comparison to tidal heat flow models.* (Preprint on Arxiv, `https://doi.org/10.48550/arXiv.2308.05717`) doi: 10.48550/arXiv.2308.05717

Rathbun, J. A., Spencer, J. R., Lopes, R. M., & Howell, R. R. (2014). Io's active volcanoes during the New Horizons era: insights from New Horizons imaging. *Icarus*, *231*, 261–272. doi: 10.1016/j.icarus.2013.12.002

Rathbun, J. A., Spencer, J. R., Tamppari, L. K., Martin, T. Z., Barnard, L., & Travis, L. D. (2004). Mapping of Io's thermal radiation by the Galileo photopolarimeter-radiometer (PPR) instrument. *Icarus*, *169*(1), 127–139. doi: 10.1016/j.icarus.2003.12.021

Schenk, P., Hargitai, H., Wilson, R., McEwen, A., & Thomas, P. (2001). The mountains of Io: Global and geological perspectives from Voyager and Galileo. *Journal of Geophysical Research: Planets*, *106*(E12), 33201–33222. doi: 10.1029/2000JE001408

Schubert, G., Anderson, J. D., Spohn, T., & McKinnon, W. B. (2004). Jupiter: the planet, satellites, and magnetosphere. In F. Bagenal, T. E. Dowling, & W. B. McKinnon (Eds.), (Vol. 2, p. 281). Cambridge University Press.

Segatz, M., Spohn, T., Ross, M. N., & Schubert, G. (1988). Tidal dissipation, surface heat flow, and figure of viscoelastic models of io. *Icarus*, *75*(2), 187–206. doi: 10.1016/0019-1035(88)90001-2

Simonelli, D. P., Dodd, C., & Veverka, J. (2001). Regolith variations on Io: Implications for bolometric albedos. *Journal of Geophysical Research: Planets*, *106*(E12), 33241–33252. doi: 10.1029/2000JE001350

Soderlund, K. (2019). Ocean dynamics of outer solar system satellites. *Geophysical Research Letters*, *46*(15), 8583–9299. doi: 10.1029/2018GL081880

Soderlund, K., Lemasquerier, D., & Bierson, C. (2023). Europa's ocean translates interior tidal heating patterns to the ice-ocean boundary. In *53rd Lunar and Planetary Science Conference.*

Spencer, D. C., Katz, R. F., & Hewitt, I. J. (2021). Tidal controls on the lithospheric thickness and topography of Io from magmatic segregation and volcanism modelling. *Icarus*(in press). doi: 10.1016/j.icarus.2021.114352

Steinke, T., Hu, H., Höning, D., van der Wal, W., & Vermeersen, B. (2020a). Tidally induced lateral variations of Io's interior. , *335*. doi: 10.1016/j.icarus.2019.05.001

Steinke, T., van Sliedregt, D., Vilella, K., van der Wal, W., & Vermeersen, B. (2020b). Can a combination of convective and magmatic heat transport in the mantle explain Io's volcanic pattern? *Journal of Geophysical Research: Planets*, *125*(12). doi: 10.1029/2020JE006521

Tackley, P. J. (2001). Convection in Io's asthenosphere: redistribution of nonuniform tidal heating by mean flows. *Journal of Geophysical Research: Planets*, *106*(E12), 32971–32981. doi: 10.1029/2000JE001411

Tackley, P. J., Schubert, G., Glatzmaier, G. A., Schenk, P., Ratcliff, J. T., & Matas, J.-P. (2001). Three-dimensional simulations of mantle convection in Io. *Icarus*, *149*(1), 79-93. doi: 10.1006/icar.2000.6536

Turcotte, D., & Schubert, G. (2014). *Geodynamics* (3rd ed.). Cambridge University Press, Cambridge (UK).

Tyler, R. H., Henning, W. G., & Hamilton, C. W. (2015). Tidal heating in a magma ocean within Jupiter's moon Io. *The Astrophysical Journal*, *218*(2), 22. doi: 10.1088/0067-0049/218/2/22

Veeder, G. J., Matson, D. L., Johnson, T. V., Blaney, D. L., & Goguen, J. D. (1994). Io's heat flow from infrared radiometry: 1983-1993. *Journal of Geophysical Research: Planets*, *99*, 17095–17162. doi: 10.1029/94JE00637

Io's Long-Wavelength Topography as a Probe for a Subsurface Magma Ocean

S. Gyalay[1] and F. Nimmo[1]

[1]University of California, Santa Cruz

Key Points:

- Maximum variation in topography implies low spatial variation in Io's tidal heating when assuming Airy isostasy.
- Tidal heat produced in a convecting aesthenosphere can reduce spatial variation in tidal heating, but requires prohibitively low viscosity.
- Io's topography is consistent with expected tidal heating spatial variations if thermal expansion drives crustal density variations.

Corresponding author: Szilárd Gyalay, sgyalay@seti.org

Abstract

We investigate how spatial variations in tidal heating affect Io's isostatic topography at long wavelengths. The difference between the hydrostatic shape implied by Io's gravity field and its observed global shape is less than the latter's 0.3 km uncertainty. Assuming Airy isostasy, degree-2 topography < 300 m amplitude is only possible if surface heat flux varies spatially by $< 17\%$ of the mean value. This is consistent with Io's volcano distribution and is possible if tidal heat is generated within a convecting layer underneath the lithosphere. However, that layer would require a viscosity $< 10^{10}$ Pa s. A magma ocean would have low enough viscosity but would not generate enough tidal heat internally. Conversely, assuming Pratt isostasy, we find $\sim$150 m degree-2 topography is easily achievable. If a magma ocean was present, Airy isostasy would dominate; we therefore conclude that Io is unlikely to possess a magma ocean.

Plain Language Summary

As it orbits Jupiter elliptically, the difference in gravitational pull experienced by the moon Io results in tidal heating due to internal friction. Some evidence suggests this heat forms a magma ocean beneath Io's crust. If so, there would be a difference in the amount of heat generated at Io's equator versus its poles and would alter the thickness of Io's crust between the two locales. Assuming the crust has a uniform density, its thickness would be inversely proportional to the tidal heat beneath the crust, which in turn affects the difference in Io's radius at the equator versus at its poles. However, reasonable variation in tidal heating across Io would result in a greater difference in radius than is observed. The difference in observed radius is more likely if variation in tidal heat across Io affects crustal density rather than crustal thickness. Then, it is more likely that Io does not have a magma ocean.

1 Introduction

It is presently a mystery whether Jupiter's hyper-volcanic satellite, Io, hides a magma ocean beneath its lithosphere (e.g., de Kleer et al., 2019; Matusyama et al., 2022). Potential evidence for such a magma ocean includes a magnetic induction signal measured by the Galileo spacecraft mission; however, such a signal could also be indicative of a magmatic sponge layer that is a mix of rock and melt (Khurana et al., 2011). Moreover, the distribution of volcanoes on Io's surface may be indicative of a concentration of tidal dissipation in the shallow mantle (e.g., Tackley et al., 2001; Tyler et al., 2015). Miyazaki and Stevenson (2022) argue such a distribution could instead be the result of heterogeneities in lithospheric weakness, as the presence of a magma ocean may redistribute any spatial variations in tidal heating due to said magma ocean. Further, they argue that a partial-melt layer within Io's subsurface is inherently unstable and would instead separate into a solid and liquid phase (Miyazaki & Stevenson, 2022). The presence of a magma ocean within Io's subsurface would have implications for the distribution and transport of tidal heating within the satellite (e.g., Matusyama et al., 2022).

In recent work, Gyalay and Nimmo (2023) demonstrated how to use the observed long-wavelength topography of Saturn's icy satellites to infer the tidal heating distribution beneath their ice shells, which provides an indirect window into their interior structure. We first investigate if such a methodology may be applied to Io by assuming Io's degree-2 shape is a combination of its hydrostatic shape (due to Io's rotational flattening and tidal buldge) and topographic variations due to the spatial pattern of tidal heating. Upon subtraction of Io's hydrostatic shape, however, we find the remnant topography is lower than the uncertainty in Io's global shape (see Section S2 of Supplement 1). While we thus cannot meaningfully apply the methodology of Gyalay and Nimmo (2023a), the uncertainty nonetheless places a useful upper bound on the amplitude of topography that spatial variations tidal heating may produce. We use this constraint to make a prediction on the presence or absence of a magma ocean that may be confirmed by upcoming Juno flybys (Keane et al., 2022). In particular, we find that Airy isostasy produces topographic amplitudes that are too large, while Pratt isostasy does not. Since Airy isostasy is likely to dominate if a magma ocean is present, we conclude that Io probably lacks a magma ocean.

2 Background

The spatial variation of tidal heating across a satellite depends greatly on the depth or thickness of the tidal-heat-producing region (e.g., the crust, lithosphere, aesthenosphere, etc.), whether the tidal-heat-producing region overlies a more rigid (e.g., rocky mantle) or a more fluid (e.g., magma ocean) layer, and whether the tides are caused by the satellite's eccentricity (orbit's ellipticity) or obliquity (tilt of the satellite's spin axis relative to the normal of its orbital plane) (e.g., Segatz et al., 1988; Beuthe, 2013). In recent work, Gyalay and Nimmo (2023a) demonstrated the use of the observed long-wavelength topography of Saturn's icy satellites to infer the tidal heating distribution beneath their ice shells.

In principle, a similar methodology could be applied to Io's topography in order to test whether it was the result of spatial variations in tidal heating consistent with a magma ocean beneath Io's lithosphere.

Previous studies have investigated the link between Io's tidal heating and its lithospheric thickness (Steinke et al., 2020a; Spencer et al., 2021), where the lithospheric thickness can be related to topography under the assumption of isostasy (see the next section, Section 3). The average surface heat flow of Io is at least 2 W m^{-2} (Veeder et al., 1994; Simonelli et al., 2001; McEwen et al., 2004; Rathbun et al., 2004; de Kleer et al., 2019). This significant quantity of heat is generated frictionally by tidal stresses as a result of Io's Laplace resonance with Europa and Ganymede (predicted by Peale et al., 1979, mere weeks before Voyager 1's flyby). This tidal heating vastly dominates the surface heat flow, which would be only 0.016 W m^{-2} if Io's entire mass had the radioactive heat production rate of Earth's mantle (7.38 pW kg^{-1}, e.g., Turcotte & Schubert, 2014). As Io's core is not radioactive, even that value is an upper bound.

If tidal heat were simply conducted to the surface, the lithosphere would need to be less than a few km thick (e.g., O'Reilly & Davies, 1981). However, Io's surface is dotted with mountains that can reach heights > 10 km (e.g., Carr et al., 1979, 1998; Schenk et al., 2001). In Section S1 of Supplement 1, we estimate that this requires a minimum lithosphere thickness of 23 km (cf. values of 14-50 km in Nash et al., 1986; Keszthelyi & McEwen, 1997; Carr et al., 1998; Jaeger et al., 2003; McEwen et al., 2004). O'Reilly and Davies (1981) argued that to satisfy the seemingly-paradoxical, observed constraints of Io's mountainous terrain and high surface heat flux, Io must advect much of its heat through a thick, cold lithosphere via heat pipes of magma that erupt upon the surface. Spencer et al. (2021) incorporated this effect into their study by using melt production from tidal dissipation to heat the lithosphere and predict surface topography. Our approach differs from theirs in a few key ways, as elaborated upon below.

We make the simplifying assumption that if tidal heating operates at the base of the lithosphere or deeper, it provides a total surface heat flux F as described by Equations 1 and 3b of O'Reilly and Davies (1981):

$$F = v\rho\left[\Delta H_f + C_p\left(T_m - T_s\right)\right] + \frac{v\rho C_p\left(T_m - T_s\right)}{e^{vd/\kappa} - 1}, \quad (1)$$

where v is the resurfacing rate, ρ is the magma density, ΔH_f is the latent heat of fusion, C_p is the specific heat, T_m is the melting temperature, T_s is the surface temperature, κ

Table 1. Variables and their (Preferred) Values

	Variable	(Pref.) Value	Note
F	Surface heat flux	$F_0 > 2$ W m^{-2}	Observed[a]
d	Lithosphere thickness	$d_0 > 23$ km	Section S1 of Supplement 1
v	Volcanic emplacement rate	$v_0 > 10.7$ mm yr^{-1} $\left(v_0 > 0.34 \text{ nm s}^{-1}\right)$	Eq. 1 for $d = 23$ km, $F = 2$ W m^{-2}
ρ	Magma density	3,000 kg m^{-3}	O'Reilly and Davies (1981)
$\Delta\rho$	Density contrast	300 kg m^{-3}	
ΔH_f	Latent heat of fusion	450 kJ kg^{-1}	O'Reilly and Davies (1981)
C_p	Specific heat	1 kJ kg^{-1} K^{-1}	O'Reilly and Davies (1981)
T_s	Surface temperature	110 K	Rathbun et al. (2014)
T_m	Melting temperature	$T_m - T_s = 1,500$ K	O'Reilly and Davies (1981)
k	Thermal conductivity	3 W m^{-1} K^{-1}	O'Reilly and Davies (1981)
κ	Thermal diffusivity	10^{-6} m^2 s^{-1}	O'Reilly and Davies (1981)
α	Volumetric thermal expansivity	3×10^{-5} K^{-1}	
Q_A	Activation energy	300 kJ mol^{-1}	
R_G	Universal gas constant	8.3 J mol^{-1} K^{-1}	
R_0	Io radius	1,800 km	Observed
g	Surface gravity	1.8 m s^{-2}	Observed
C	Moment of Inertia	$0.3782\ M\ R_0^2$	Schubert et al. (2004)

[a]Veeder et al. (1994); Simonelli et al. (2001); McEwen et al. (2004); Rathbun et al. (2004); de Kleer et al. (2019)

is the thermal diffusivity, and d the lithospheric thickness. One can also find the thermal conductivity of the lithosphere k as $k = \rho C_p \kappa$. Table 1 lists our preferred values for these variables, which borrow largely from O'Reilly and Davies (1981). The first term on the right-hand side of Equation 1 provides the portion of heat flux that is advected through heat pipes to the surface, while the second term provides the portion of heat flux that is conducted through the lithosphere. In the limit of low volcanic emplacement v, we recover Fourier's law of thermal conduction through a slab.

At a given lithospheric thickness, Equation 1 implies a larger volcanic emplacement rate produces a higher heat flux; while for a given resurfacing/emplacement rate, the lithosphere thins when tidal dissipation increases. The latter point can also be seen by inverting Equation 1 to solve for d,

$$d = \frac{\kappa}{v} \ln\left(\frac{v\rho C_p \left(T_m - T_s\right)}{F - v\rho \left[\Delta H_f + C_p \left(T_m - T_s\right)\right]} + 1 \right). \tag{2}$$

Equation 1 or 2 only satisfies both the minimum average surface heat flux $F > 2$ W m^{-2} and our minimum average lithosphere thickness $d > 23$ km for Io when the conductive heat flux is a small fraction of the total heat flux, $F_{cond} < 3 \times 10^{-4} F$. Alternatively, one may simply state that the total heat flux is dominated by the advective term, $F \sim F_{adv}$. This requires an average volcanic emplacement rate of $v = 10.7$ mm yr^{-1} (3.4×10^{-10} m s^{-1}) when $F = 2$ W m^{-2}.

By inferring the spatial distribution of tidal heating from topography, we may make inferences about the interior structure of Io. But first we must isolate the portion of Io's topography that arises from variations in tidal heating. Tidal heating varies spatially in even-orders of spherical harmonic degrees 2 and 4. We would thus wish to analyze Io's topography in those same spherical harmonics (e.g., Gyalay & Nimmo, 2023a). Unfortunately, we find in Section S2 of Supplement 1 that after accounting for the hydrostatic component of Io's shape (i.e., that which is due to Io's tidal bulge and rotational flattening), Io's remaining topography in those spherical harmonics is less than the uncertainty in global shape. Any conclusion on patterns of tidal heating inferred from this topography is then meaningless.

However, the *magnitude* of topographic variation may still yield some important constraints. In our case, the maximum (non-hydrostatic) topographic variation is limited by the uncertainty in degree-2 shape, which is on the order of 0.3 km (Section S2 of Supplement 1). In, e.g., Beuthe (2013), the heat flux due to tidal heating can vary spatially in magnitude on the order of its average value. Io would not be as hot as it is without significant tidal heating (Peale et al., 1979). Then it stands to reason that most (if not all) of Io's heat flow is due to tidal heating. Given some variation in tidal heating, we can calculate the expected variation in Io's topography and compare it to our bounds on the possible variation in Io's topography.

3 Predicting Isostatic variation in Io's topography

We make the assumption that Io's crust is in isostatic equilibrium at long wavelengths (low spherical harmonic degree). In any form of isostasy, we expect that either the total mass or pressure at some depth to be constant across a planetary body despite variations in the topography (see, e.g., Hemingway & Masuyama, 2017, for an argument in favor of equal-pressure isostasy). An alternate treatment of isostasy seeks to minimize the deviatoric stress within the crust (Beuthe, 2021). Minimum-stress isostasy can be approximated by equal-weight isostasy, which returns results between those of equal-mass and equal-pressure isostasy. In Gyalay and Nimmo (2023a), we used both equal-mass and equal-pressure isostasy as endmember cases in examining the ice shell of Tethys. Ultimately, interpretation of Tethys' interior was consistent across both treatments of isostasy. However, as we do not expect a significantly thick lithosphere on Io relative to its total radius, constant-pressure isostasy and constant-mass isostasy are nearly identical. Therefore in this paper, we default to the simpler calculations using equal-mass isostasy.

Beyond the choice of equal-mass, equal-pressure, equal-weight, or minimum-stress isostasy, there are still two overarching types of isostasy: Airy isostasy wherein topography is due to crustal thickness variations (more likely in the case of a magma ocean) or Pratt isostasy where topography is due to crustal density variations. In this manuscript, we apply these isostatic assumptions to the entire lithosphere (i.e., both the crust *and* the uppermost layer of the mantle) rather than just the crust. We assume that the bulk density of the crust plus uppermost mantle can differ from that of the mantle beneath, because of petrological differences arising during melt production and transport. The presence of heat pipes transporting melt from the mantle to the surface further necessitate another assumption: the dependence of volcanic emplacement rate v upon variations in heat flow F. We examine two endmember states: either v is a constant value $v = v_0$, or v varies in direct proportion to the local surface heat flux $v = v_0 F/F_0$, where F_0 is the average heat flow. In comparison, Spencer et al. (2021)'s treatment of Pratt isostasy in Io's lithosphere makes the distinction between the abundance of heat pipes and the flux of melt through each heat pipe. They hold either the pipe density uniform (but allow flow to vary in each) or the flow through any pipe constant (but allow variation in the concentration of heat pipes). However, this extra flexibility requires the assumption of additional constants to relate the values to v. We avoid having to make such assumptions with our approach.

In the limit of strong tidal heating, the amplitude of heat flux variations δF in spherical harmonic degree-2 (where $\delta F = F - F_0$) approaches the average total heat flux F_0 (e.g. Beuthe, 2013). Then, we may test which of our cases predict isostatic topography as a function of spatial variations in tidal heating that is consistent with a maximum amplitude of ~ 0.3 km. We plot the expected topography as a function of heat flux variation for each mode of isostasy (Pratt or Airy) and dependence of emplacement rate on local heat flux ($v = v_0$ or $v \propto F$) in Figure 1.

3.1 Airy Isostasy

If there is a sub-surface magma ocean, we would expect Airy isostasy as with the floating shells of icy satellites. Here, we assume the topography is driven by variations in lithospheric thickness. To maintain a constant pressure at depth, lithospheric thinning would result in negative surface topography, and vice versa. We can relate topography h to a change in lithospheric thickness δd:

$$h = \frac{\delta d}{\left(1 + \frac{\rho}{\Delta\rho}\right)}, \tag{3}$$

where $\Delta\rho$ is the density contrast between the lithosphere and the underlying material. If the magma is sourced from the upper mantle and is denser than the lithosphere, a topographic high is the result of a thicker lithosphere. If instead the magma is sourced from the base of the crust and is less dense than the lithosphere (as a whole), then this equation implies a topographic high is the result of a thinner lithopshere. However, that latter scenario is inherently unstable and subject to overturn of the lithosphere. We therefore assume the lithosphere is 300 kg m^{-3} less dense than the magma.

3.1.1 Constant v case

If we assume the emplacement rate v is uniform across Io's surface in the case of Airy isostasy, we can begin with Equation 2 to calculate the expected topography h for some given variation in heat flux δF from the mean F_0. After setting $v = v_0$, the difference in lithospheric thickness δd calculated by subtracting the mean d_0 from Equation 2 is,

$$\delta d = \frac{\kappa}{v_0} \ln\left(\frac{v_0 \rho C_p \left(T_m - T_s\right)}{F_0 + \delta F - v_0 \rho \left[\Delta H_f + C_p \left(T_m - T_s\right)\right]} + 1\right) - d_0. \tag{4}$$

Note that $v_0 \rho \left[\Delta H_f + C_p \left(T_m - T_s\right)\right]$ is the advective heat flux, F_{adv}. Then,

$$\delta d = \frac{\kappa}{v_0} \ln\left(\frac{v_0 \rho C_p \left(T_m - T_s\right) \frac{1}{F_0}}{1 + \frac{\delta F}{F_0} - \frac{F_{adv}}{F_0}} + 1\right) - d_0. \tag{5}$$

Then because the conductive heat flux $F_{cond} = v\rho C_p \left(T_m - T_s\right) / \left(e^{vd/\kappa} - 1\right)$, we may further rearrange the equation and substitute δd into Equation 3 to find,

$$h = \frac{1}{1 + \frac{\rho}{\Delta\rho}} \left[\frac{\kappa}{v_0} \ln\left(\frac{\frac{F_{cond,0}}{F_0} e^{v_0 d_0/\kappa} + \frac{\delta F}{F_0}}{\frac{F_{cond,0}}{F_0} + \frac{\delta F}{F_0}}\right) - d_0\right], \tag{6}$$

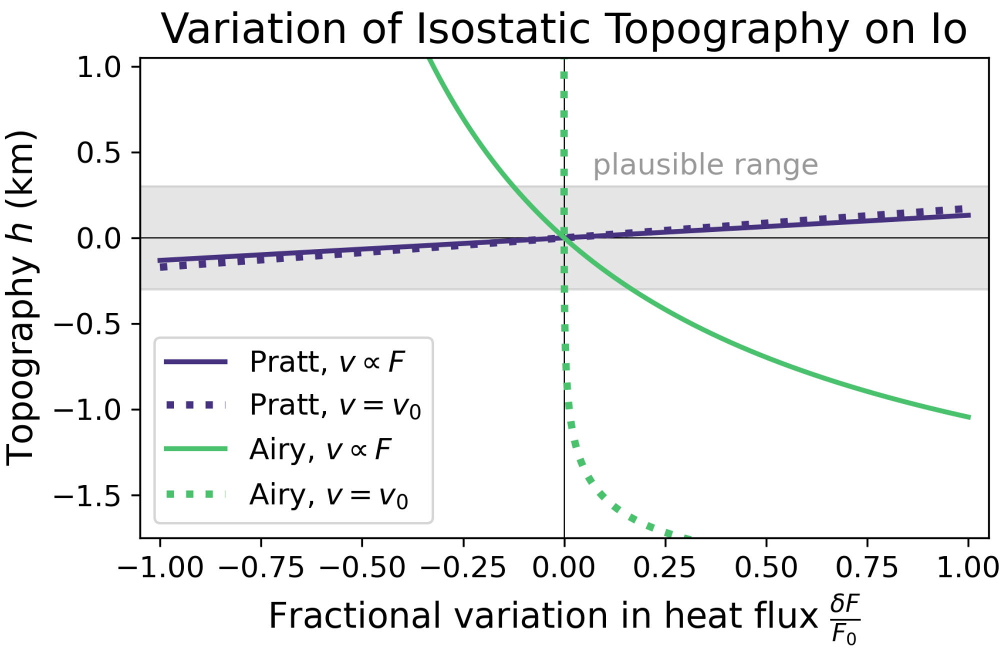

Figure 1. We plot the variation of Io's isostatic long wavelength topography as a function of heat flux, as compared to the amplitude of topography $|h| < 0.3$ km allowed by the uncertainty in Io's global shape (gray region). Topography that assumes Airy isostasy and $v = v_0$ (dotted green line) is characterized by Equation 6 for $F_{cond,0} = 2.95 \times 10^{-4} F_0$, which is the maximum value allowed for the minimum average lithospheric thickness $d_0 = 23$ km and minimum average heat flux $F_0 = 2$ W m^{-2}. Increasing d_0 would further limit $F_{cond,0}$ and the maximum variability of δF. Topography that assumes Airy isostasy and $v \propto F$ (solid green line) is characterized by Equation 8 for minimum average lithospheric thickness $d_0 = 23$ km. Larger d_0 would increase topography as a function of heat flux variation. Topography that assumes Pratt isostasy and $v = v_0$ (dotted purple line) is characterized by Equation 21 for minimum average volvanic emplacement $v_0 = 10.7$ mm yr^{-1}. Topography that assumes Pratt isostasy and $v \propto F$ is characterized by Equation 28 for the same assumed v_0. Larger v_0 would reduce variation in h for both cases of Pratt isostasy. All other parameters use the preferred values in Table 1.

where $F_{cond,0}$ is F_{cond} at $d = d_0$ and $v = v_0$. Because F_{adv} remains constant if $v = v_0$, then $|\delta F| < F_{cond,0}$, where $F_{cond,0} < 3{\times}10^{-4}$ for the preferred value of our parameters in Table 1. Further, in Equation 6 we can easily see that the topography is undefined if $\delta F = -F_{cond,0}$. Thus, it is impossible for tidal heat flux variations on the order of the average heat flux $|\delta F| \sim F_0$ to exist for an Io lithosphere under Airy isostasy with constant emplacement rate v_0 unless the total heat flux were dominated by the conductive term.

3.1.2 $v \propto F$ case

When v is instead proportional to F in the case of Airy isostasy, we substitute $v = v_0 F/F_0$ into Equation 1 and solve for F:

$$F = \frac{F_0}{d}\frac{\kappa}{v_0}\ln\left(\frac{v_0\rho C_p(T_m - T_s)}{F_0 - v_0\rho[\Delta H_f + C_p(T_m - T_s)]} + 1\right). \tag{7}$$

When compared to Equation 2, we may simplify Equation 7 to $Fd = F_0 d_0$. Substituting $d = d_0 + \delta d$ and Equation 3 into Equation 7, we rearrange and find

$$h = \frac{-d_0}{\left(1 + \frac{\rho}{\Delta\rho}\right)}\frac{\frac{\delta F}{F_0}}{\left(1 + \frac{\delta F}{F_0}\right)}. \tag{8}$$

When $|\delta F| \sim F_0$ we should expect the amplitude of topography h in degree-2 to reach about $d_0/20$. If $h \leq 0.3$ km, then this is only true when $d_0 \leq 6$ km—which is thinner than the $\sim$ 23 km minimum average thickness we expect for Io's lithosphere (Section S1 of Supplement 1).

3.2 Pratt Isostasy

Under Pratt isostasy, we expect topography to be the result of density variations in the lithosphere. Traditionally, Pratt isostasy also assumes the base of the lithosphere is "flat" and there is no basal topography. For Io, this is less certain (cf., Spencer et al., 2021), but as a combination of Pratt and Airy would be dominated by the effects of Airy isostasy, we assume this traditionally flat basal topography as an endmember case. To maintain constant pressure at depth, density variations in the lithosphere $\delta\rho$ from a reference average lithospheric density ρ_0 are

$$\delta\rho = -\rho_0\frac{h}{d_0}. \tag{9}$$

Assuming density variations are due only to thermal expansion or contraction of the lithosphere, we relate the change in crustal density to the change in the lithosphere's average temperature $\delta\bar{T}$ from some reference temperature $\bar{T}_0$ for a thermal expansivity α:

$$\delta\bar{T} = -\frac{\delta\rho}{\alpha\rho_0} = \frac{\delta d}{\alpha d_0} = \frac{h}{\alpha d_0}, \tag{10}$$

where the final equality makes use of the fact that $\delta d = h$ in Pratt isostasy. It then behooves us to calculate the average temperature of the lithosphere and relate it to the heat flux through the lithosphere. O'Reilly and Davies (1981) provide the temperature profile as a function of depth z (where $z = 0$ is the surface, and $z = d$ is the base of the lithosphere):

$$T(z) = T_s + (T_m - T_s)\frac{e^{vz/\kappa} - 1}{e^{vd/\kappa} - 1}. \tag{11}$$

By taking the integral of Equation 11, we can find the average temperature of the lithosphere:

$$\bar{T} = \frac{1}{d}\int_0^d T(z)\,dz, \tag{12}$$

Finding

$$\bar{T} = T_s + (T_m - T_s)\Big(\frac{\kappa}{vd} - \frac{1}{e^{vd/\kappa} - 1}\Big), \tag{13}$$

which agrees that for high emplacement rates or thick lithospheres, most heat transport is accomplished by the advection of magma and thus the lithosphere's average temperature will be closer to the the surface temperature than the melting temperature. If v or d approaches 0, we can take the approximation $e^{vd/\kappa} \approx 1+\frac{vd}{\kappa}+\frac{1}{2}(\frac{vd}{\kappa})^2$ and we find that $\bar{T}$ approaches $(T_m - T_s)/2$, which is what we expect in the case without heat pipes. Spencer et al. (2021) also assume Pratt isostasy in Io's lithosphere would be dominated by thermal expansion.

In our study, we explicitly vary the volcanic emplacement rate v and lithospheric thickness d, but hold the surface temperature T_s constant. T_m can vary in some unknown manner, so in our formalism for translating the topography δd into heat flux F via Pratt isostasy, we want to eliminate the dependence of T_m before we continue our derivation. We can rearrange Equation 13 to find

$$T_m - T_s = \frac{\bar{T} - T_s}{\frac{\kappa}{vd} - \frac{1}{e^{vd/\kappa}-1}}. \tag{14}$$

Substituting Equation 14 into Equation 1 and rearranging, we find

$$F = v\rho\left[\Delta H_f + \frac{vd}{\kappa}(\bar{T} - T_s)\frac{e^{vd/\kappa}}{e^{vd/\kappa} - 1 - \frac{vd}{\kappa}}\right]. \tag{15}$$

For our minimum values of v, d, and F (Table 1), vd/κ is at minimum 7.8; implying $e^{vd/\kappa} > 2400$. Then, the fraction $e^{vd/\kappa}/\left(e^{vd/\kappa} - 1 - \frac{vd}{\kappa}\right)$ is only greater than unity by a maximum of 0.4%, meaning we may safely neglect the fraction for our consideration of Pratt isostasy. Simpler now, we find,

$$F \approx v\rho \left[\Delta H_f + \frac{vd}{\kappa} C_p (\bar{T} - T_s) \right]. \tag{16}$$

3.2.1 Constant v case

If we assume emplacement rate v is uniform across Io's surface in the case of Pratt isostasy, we can substitute $v = v_0$ into Equation 16. Then, one would expect the difference in heat flux from average δF to be

$$\delta F \approx \frac{v_0^2 \rho C_p}{\kappa} [d_0 \delta\bar{T} + h(\bar{T}_0 - T_s) + h\delta\bar{T}]. \tag{17}$$

When we substitute $\delta\bar{T} = h/(\alpha d_0)$ (Equation 10) into Equation 17, we find the variation in heat flux through Io's lithosphere under Pratt isostasy and constant volcanic emplacement $v = v_0$ as,

$$\delta F \approx \frac{v_0^2 h \rho C_p}{\kappa} \left[\frac{1}{\alpha} \left(1 + \frac{h}{d_0} \right) + \left(\bar{T}_0 - T_s \right) \right]. \tag{18}$$

In the first term within the square brackets, we expect $\frac{h}{d_0} \ll 1$, meaning we can drop the second term within those parentheses for this approximation. A reasonable volumetric thermal expansivity for rock at $\bar{T}$ is $\alpha \sim 3 \times 10^{-5}$ K^{-1}, meaning that $\bar{T}_0 - T_s \ll \alpha^{-1}$, and we may drop that second term. Thus, our relationship between topography h and variation in tidal heating δF can be reduced to,

$$\delta F \simeq \frac{v_0^2 \rho C_p}{\kappa \alpha} h. \tag{19}$$

Keeping in mind that $F_0 \sim F_{adv}$, we can account for variations in F as a factor of itself by dividing both sides of Equation 19 by F_0 or F_{adv},

$$\frac{\delta F}{F_0} \sim h \frac{v_0}{\kappa} \frac{C_p \frac{1}{\alpha}}{\Delta H_f + C_p (T_m - T_s)}. \tag{20}$$

Solving now for the topography h,

$$h \sim \frac{\delta F}{F_0} \frac{\kappa}{v_0} \alpha \left[\frac{\Delta H_f}{C_p} + (T_m - T_s) \right]. \tag{21}$$

If heat flux varies on the order of itself ($|\delta F| \sim F_0$), then we expect the amplitude of h to reach about $h \sim 172$ m $\times \frac{\delta F}{F_0} \frac{10.7 \text{ mm yr}^{-1}}{v_0}$ (where $v_0 = 10.7$ mm yr^{-1} is the minimum average volcanic emplacement expected for the minimum observed average heat flux of

$F \sim 2$ W m^{-2}), which would create long-wavelength topography *less* than the maximum possible degree-2 topography (as limited by our uncertainty, Section S2 of Supplement 1).

3.2.2 $v \propto F$ case

When v is instead proportional to F in the case of Pratt isostasy, we substitute $v = v_0 F/F_0$ into Equation 16 and rearrange to find

$$\frac{F}{F_0} \approx \frac{F_0 - v_0 \rho \Delta H_f}{\frac{v_0 d}{\kappa} v_0 \rho C_p \left(\bar{T} - T_s\right)}. \tag{22}$$

In this case, the variation in F is due to variation in the $1/[d(\bar{T} - T_s)]$ term. Neither d nor $\bar{T}$ are expected to vary greatly, and thus we make the approximation

$$\delta\left[\frac{1}{d\left(\bar{T} - T_s\right)}\right] \simeq -\frac{\left[d_0 \delta\bar{T} + h\left(\bar{T}_0 - T_s\right)\right]}{d_0^2 (\bar{T}_0 - T_s)^2}. \tag{23}$$

Thus,

$$\frac{\delta F}{F_0} \simeq -\frac{\left(F_0 - v_0\rho\Delta H_f\right)\left[d_0\delta\bar{T} + \delta d\left(\bar{T}_0 - T_s\right)\right]}{v_0^2 d_0^2 k \left(\bar{T}_0 - T_s\right)^2}. \tag{24}$$

When we substitute $\delta\bar{T} = h/\left(\alpha d_0\right)$ (Equation 10) into Equation 24, we find the variation in heat flux through Io's lithosphere under Pratt isostasy and volcanic emplacement rate proportional to heat flux variations $v = v_0 F/F_0$ as,

$$\frac{\delta F}{F_0} \simeq -\frac{\left(F_0 - v_0\rho\Delta H_f\right)\left[\frac{1}{\alpha} + \left(\bar{T}_0 - T_s\right)\right] h}{v_0^2 d_0^2 k \left(\bar{T}_0 - T_s\right)^2}. \tag{25}$$

Then, using Equation 14, the $\bar{T}_0 - T_s$ term within the square brackets can be substituted with $\bar{T}_0 - T_s = \left(T_{m,0} - T_s\right)\left[\frac{\kappa}{vd} - \frac{1}{\exp\left(vd/\kappa\right) - 1}\right]$. Assuming $T_m - T_s = 1{,}500$ K, this term is a *maximum* of 193 K (for our minimum v_0 and d). Meanwhile, α^{-1} is *always* much greater than $\left(\bar{T}_0 - T_s\right)$. Thus, our relationship between topography and variation in tidal heating δF can be reduced to,

$$\frac{\delta F}{F} \sim \frac{F_0 - v_0\rho\Delta H_f}{\frac{v_0 d_0}{\kappa} v_0 \rho C_p \left(\bar{T}_0 - T_s\right)} \times \frac{-1}{\alpha\left(\bar{T}_0 - T_s\right)} \frac{h}{d_0}. \tag{26}$$

If one substitutes $\bar{T}_0 - T_s$ with Equation 10, they will find the denominator of the first fraction in Equation 26 will very nearly be equivalent to $F_0 - v_0\rho\Delta H_f$ (Equation 1) and thus reduce the fraction to 1. Then,

$$\frac{\delta F}{F_0} \sim -\frac{v_0}{\kappa}\frac{h}{\alpha\left(T_{m,0} - T_s\right)}. \tag{27}$$

Finally, rearranging to solve for h,

$$h \sim \frac{\delta F}{F_0} \frac{\kappa}{v_0} \alpha \left(T_m - T_s\right). \tag{28}$$

If heat flux varies on the order of itself ($|\delta F| \sim F_0$), then we expect the amplitude of h to reach about $h \sim 132$ m $\times \frac{\delta F}{F_0} \frac{10.7 \text{ mm yr}^{-1}}{v_0}$.

4 Implications and Discussion

Should Io have a magma ocean, we might expect its lithosphere to experience Airy isostasy rather than Pratt isostasy. However, when assuming Airy isotasy, we find in both the constant $v = v_0$ and proportional $v \propto F$ cases of volcanic emplacement that the resulting degree-2 topography is far greater than the maximum possible topography as limited by our uncertainty (Figure 1). Thus, it is impossible for Io lithosphere's lithosphere to be in Airy isostasy if the variation in heat flux is as great as one would expect from tidal heating. Instead, this would imply that the heat flux is a mostly uniform background. Io cannot generate this much heat radioactively, so if Io were in Airy isostasy, some additional process would need either to erase either Io's topography in response to strong tidal heat variations *or* any spatial variation in the tidal heat that would produce this topography.

However, it *is* possible for Io to produce its expected long-wavelength topography while under strong tidal heating variations on the order of its average tidal heat flux—*if* Io's lithosphere operates under Pratt isostasy. This is true both when volcanic emplacement rate is uniform across Io's surface and when variation in volcanic emplacement rate is proportional to variations in tidal heating (Figure 1). In both cases, we expect the amplitude of degree-2 topography to reach about ~ 150 m when average volcanic emplacement rate v is that which is expected for the observed minimum average heat flow (Table 1).

Before eliminating the possibility of Airy isostasy, we explore the reasons why there may not be significant topography in response to expected variations of tidal heating.

4.1 Topographic relaxation

One reason why Io might not have significant topography if it were in Airy isostasy could be lower crustal (here, lithospheric) flow. The warmest portion of the lithosphere will tend to have the lowest viscosity and will flow laterally in response to horizontal pressure gradients (e.g., McKenzie et al., 2000; Nimmo & Stevenson, 2001; Nimmo, 2004). That is, the deepest roots of the lithosphere will naturally want to smooth out and reduce its basal topography. Typically, this timescale is much longer than that for attaining isostatic topography in the first place (e.g., Nimmo & Stevenson, 2001). We examine here if this holds true for Io as well.

As for the crusts of many planetary bodies, the dynamic viscosity η of Io's lithosphere is expected to vary exponentially with its temperature, $\eta \propto \exp\left[Q_A/\left(R_G T\right)\right]$, where Q_A is the activation energy of the rock that makes up the lithosphere and R_G is the universal gas constant. Because the viscosity depends exponentially upon the temperature within the lithosphere, we expect only the base of Io's lithosphere to have a viscosity low enough to flow laterally. The thickness of this flowing region is a few times some characteristic lengthscale δ_{flow}. Then, the timescale τ_{rel} to relax (reduce) the amplitude of sinusoidal variations in topography in spherical harmonic degree l by a factor of e is provided by Nimmo (2004) as

$$\tau_{rel} = \frac{\eta_0}{\Delta\rho g}\left(\frac{R_0}{l}\right)^2 \frac{1}{\delta_{flow}^3}, \tag{29}$$

where η_0 is the reference viscosity at the base of the lithosphere (where $T = T_m$), and R_0 is Io's average radius (listed in Table 1). We focus on spherical harmonic degree $l = 2$, where the greatest variation in tidal heating is expected. At $l = 2$, the wavelength of topographic variation is half of Io's circumference.

As one might expect from a lengthscale that characterizes the thickness of the flowing region of a lithosphere when its viscosity depends exponentially on temperature, δ_{flow} depends on the vertical temperature gradient $\frac{\partial T}{\partial z}$ at the base of the lithosphere, where z is depth measured from Io's surface. Following Nimmo and Stevenson (2001), if viscosity depends on temperature as $\eta \sim e^{Q_A/(R_G T)}$ and the temperature gradient at some distance $\Delta z = d - z$ above the base of the lithosphere (thickness d) is approximately linear, then

$$\exp\left(\frac{Q_A}{R_G T}\right) \approx \exp\left(\frac{Q_A}{R_G T_m}\right)\exp\left(\frac{\Delta z}{\delta_{flow}}\right). \tag{30}$$

Thus,

$$\delta_{flow} \simeq \frac{R_G}{Q_A}\frac{T_m^2}{\left.\frac{\partial T}{\partial z}\right|_{z=d}} \tag{31}$$

(cf., Nimmo & Stevenson, 2001; Nimmo, 2004).

Were Io's lithosphere to be in a purely conductive regime (very thin crust), we would find $\delta_{flow} = R_G k T_m^2/\left(Q_A F_{cond}\right)$. However, because we expect Io to have a lithospheric thickness $d > 23$ km (Section S1 of Supplement 1), we must instead take the derivative of Equation 11 to find

$$\delta_{flow} = \frac{R_G}{Q_A} \frac{\kappa}{v} \frac{T_m^2}{(T_m - T_s)}. \tag{32}$$

This is substantially smaller than what one expects in a purely conductive regime, by a factor of about $3F_{adv}/(4F_{cond})$. This is because the temperature profile we expect in Io's lithosphere (Equation 11) is relatively close to the surface temperature T_s until $z \to d$ and the temperature exponentially climbs to T_m. Assuming Io's lithosphere has an activation energy of ~ 300 kJ mol^{-1}, δ_{flow} is only about 100 m.

Such a low δ_{flow} vastly increases the amount of time it would take to relax Io's isostatic topography. Meanwhile, the timescale to attain topography in isostatic equilibrium τ_{iso} is $\tau_{iso} \sim \eta_M l/(2\pi\rho_M g R_0)$ (Nimmo & Stevenson, 2001), where η_M is mantle viscosity and ρ_M is mantle density. Then, a comparison of the two timescales yields

$$\frac{\tau_{rel}}{\tau_{iso}} = 2\pi \frac{\eta_0}{\eta_M} \frac{\rho_M}{\Delta\rho} \left(\frac{R_0}{\delta_{flow} l} \right)^3, \tag{33}$$

where with our preferred values (Table 1) is about 10^{14} η_0/η_M. This means that for lower crustal flow to reasonably erase any long-wavelength topography due to variations in tidal heating, Io's mantle would need to be 10^{11} times more viscous than the base of its lithosphere. While the viscosity profile of Io is poorly constrained (cf., Lainey et al., 2009; Bierson & Nimmo, 2016; Steinke et al., 2020a, 2020b; Spencer et al., 2021), such a contrast sparks incredulity. Thus, it is unlikely that in the event of Airy isostasy, topography would be subdued by lower lithospheric flow.

4.2 Tidal heat redistribution

Another possibility to investigate is the redistribution of tidal heat flux into a more uniform heating pattern. Assuming the case where volcanic emplacement rate $v \propto F$, we may rearrange Equation 8 to find

$$\frac{|\delta F|}{F_0} = \frac{1}{1 + \frac{d_0}{h\left(1 + \frac{\rho}{\Delta\rho}\right)}}. \tag{34}$$

For maximum degree-2 topography of $h \sim 0.3$ km (Section S2 of Supplement 1) and minimum lithosphere thickness of $d_0 \sim 23$ km (Section S1 of Supplement 1), we find that variations in heat flux must have a maximum $|\frac{\delta F}{F_0}| < 0.17$ to not violate the observed topography (see also Figure 1). By examining the volcano distribution, Steinke et al. (2020b) find that the magnitude of degree-2 coefficients of volcano density vary from

0.02 to 0.146× the average volcano density, which is consistent with our finding that degree-2 variations in heat flux are below 0.17 of the average. Hamilton et al. (2013) likewise argue that if Io's volcano distribution is related to a tidal heat distribution, then that heating pattern is approximately 20% tidal heating in Io's aesthenosphere with the rest either a uniform heat distribution or deep mantle heating. As less than 1% of Io's total heat production is radiogenic, then a uniform heat distribution would need to have been a tidal heating pattern that was blurred into appearing uniform.

The observed variation in surface heat flux δF_O may be related to the originally produced heat flux δF_P by some blurring function $B(l)$ that depends on the spherical harmonic degree l (e.g., Steinke et al., 2020a, 2020b). This assumes that there exists a convective layer beneath the lithosphere (typically the asesthenosphere) that produces its own heat tidally. Following Tackley (2001); Steinke et al. (2020a, 2020b), we find this blurring function to be

$$B\left(l\right) = \frac{R_0 \pi}{l d_{conv}} C_B \mathrm{Ra}_H^{-\beta}, \tag{35}$$

where d_{conv} is the thickness of the convecting layer, C_B and β are constants related to the blurring of the heat flux variations, and Ra_H is the Rayleigh-Roberts number (sometimes referred to as the internal-heating Rayleigh number), which characterizes the convective transport of heat-producing material as compared to the diffusion of its heat and is defined as

$$\mathrm{Ra}_H = \frac{\rho g \alpha H d_{conv}^5}{k \eta_{conv} \kappa}, \tag{36}$$

where H is the thermal productivity in the mantle in units of power per mass and η_{conv} is the dynamic viscosity of the convecting layer. Following Steinke et al. (2020a, 2020b), we approximate $H = f_{cc} F_P / d_{conv}$, where f_{cc} is the fraction of tidal heating produced in the convective layer F_P that is transported through the mantle by conduction and convection (as opposed to bouyant magmatism through the mantle).

In order for the spatial distribution of volcano density to resemble a tidal heating pattern whose heat flux varies approximately $\leq 17\%$ of the average heat flow, then $B(2) \leq 0.17$. That is,

$$\mathrm{Ra}_H \geq \left(\frac{R_0}{d_{conv}} \frac{\pi}{2} \frac{C_B}{0.17} \right)^{1/\beta}. \tag{37}$$

When heating is uniform within the convective layer, $C_B = 4.413$ and $\beta = 0.2448$, while when the heating is focused at the boundary of the layer, $C_B = 2.869$ and $\beta = 0.2105$ (Tackley, 2001). Depending on the regime then, this would mean Ra_H has to be greater than about 10^{13} to 10^{14} (assuming a convective layer thickness of 50 km) to reduce degree-2 tidal heating variations to 17%.

For constants in Table 1, we find this implies for such blurring to occur,

$$\frac{\eta_{conv}}{f_{cc}} \leq 7 \times 10^{10} \text{ Pa s} \left(\frac{F_P}{2 \text{ W m}^{-2}}\right) \left(\frac{d_{conv}}{50 \text{ km}}\right)^{4+\frac{1}{\beta}} . \tag{38}$$

Steinke et al. (2020b) find that f_{cc} is likely < 0.2. This then requires that if there were a circulating layer, its viscosity would be $< 10^{10}$ Pa s, which is lower than most estimates of asthenospheric viscosity (cf., Tackley, 2001; Steinke et al., 2020b). To achieve such a low viscosity might require the convecting layer to be a magma ocean—but then the amount of tidal heating produced within the convecting layer F_P would be greatly diminished. Furthermore, any heat produced by a magma ocean tides (e.g. Tyler et al., 2015) would be mainly due to the friction of the magma ocean dragging against the overlying lithosphere (cf. for ocean tides within icy satellites, Chen et al., 2014; Hay & Matsuyama, 2019).

The extent to which a magma ocean may instead redistribute a tidal heating pattern generated from *beneath* it rather than within it is presently unclear. However, we may draw an analogy with Europa, where it has been found that when ocean circulation has a weak dependence on rotation, such circulation has minimal effect upon the dispersion of tidal heating distributions from beneath (Soderlund et al., 2023). Thermal circulation in a potential magma ocean within Io would have an even weaker dependence on rotation, owing to the much higher viscosity of magma compared to water (a deeper discussion on how to characterize heat transfer in the circulating oceans of icy satellites may be found in Soderlund, 2019). Thus, we find it unlikely that a tidal heating pattern is redistributed by a convecting layer—whether the tidal heat is produced within a convecting aesthenosphere or produced beneath a convecting magma ocean.

5 Conclusions

Ultimately, we find that the maximum amplitude of isostatic topography that results from spatial variations in tidal heating across Io is irreconcilable with the expected spatial variation in tidal heating if we assume that Io's lithosphere operates under Airy isostasy. The amplitude of tidal heating variation in spherical harmonic degree 2 is expected to be on the order of average tidal heating. Instead, the assumption of Airy isostasy requires an amplitude of tidal heating variation $< 17\%$ of the average heat flow. A convective layer can produce and redistribute tidal heating into a relatively uniform heating pattern, but requires that this convective layer both produces most of Io's tidal heat *and* that this layer have an extremely low viscosity $< 10^{10}$ Pa s. An aesthenosphere could produce adequate internal tidal heating (i.e., not from drag at the base of the lithosphere) while a magma ocean may have a low enough viscosity, but neither possibility fulfills both conditions.

If we instead assume that Io's lithosphere operates under Pratt isostasy, then the predicted isostatic topography is consistent with the maximum allowed by the observations. Because we rule out Airy isostasy in favor of Pratt isostasy, this implies that a magma ocean is unlikely. This can soon be tested, as Juno's upcoming orbits of Jupiter will bring it close to Io. Already, recent infrared imagery has been used to analyze the distribution of Io's volcanic heat flow. Pettine et al. (2023) find that the tidal heating pattern implied by Io's volcano distribution is anti-correlated with a global magma ocean and instead suggests tidal heating in the aesthenosphere (cf., Davies et al., 2023), demonstrating a similar conclusion to our own using an entirely different dataset and method. Upcoming Juno flybys also allow the measurement of new gravitational data (Keane et al., 2022) that supplements measurements from older spacecraft. Such gravity observations could unveil Io's Love number k_2, which characterizes Io's tidal response. A high value of $k_2 \sim 0.5$ is expected if Io has a magma ocean, while a lower value $k_2 \sim 0.1$ is expected without a magma ocean (Bierson & Nimmo, 2016; de Kleer et al., 2019). Thus, we predict that if k_2 is measured for Io with Juno data, it will be low.

Open Research Section

This paper is purely theoretical, only deriving equations to apply to previously observed physical parameters. As such, no datasets were analyzed or produced for this paper. The python code used to create Figure 1 has been uploaded to the Dryad Repository and is listed in our References as Gyalay and Nimmo (2023b).

Acknowledgments

FN received funding from NASA Grant 80NSSC21K1802.

References

Beuthe, M. (2013). Spatial patterns of tidal heating. *Icarus*, *223*(1), 308–329. doi: 10.1016/j.icarus.2012.11.020

Beuthe, M. (2021). Isostasy with Love – i: elastic equilibrium. *Geophysical Journal*

International, *225*(3), 2157–2193. doi: 10.1093/gji/ggab073

Bierson, C. J., & Nimmo, F. (2016). A test for Io's magma ocean: modeling tidal dissipation with a partially molten mantle. *Journal of Geophysical Research: Planets*, *121*(11), 2211–2224. doi: 10.1002/2016JE005005

Carr, M. H., Masursky, H., Strom, R. G., & Terrile, R. J. (1979). Volcanic features of Io. *Nature*, *280*(5725), 729–733. doi: 10.1038/280729a0

Carr, M. H., McEwen, A. S., Howard, K. A., Chuang, F. C., Thomas, P., Schuster, P., ... Galileo Imaging Team (1998). Mountains and calderas on Io: Possible implications for lithosphere structure and magma generation. *Icarus*, *135*(1), 146–165. doi: 10.1006/icar.1998.5979

Chen, E. M. A., Nimmo, F., & Glatzmaier, G. A. (2014). Tidal heating in icy satellite oceans. *Icarus*, *229*, 11–30. doi: 10.1016/j.icarus.2013.10.024

Davies, A. G., Perry, J., Williams, D. A., & Nelson, D. M. (2023). *Io's polar volcanic thermal emission indicative of magma ocean and shallow tidal heating models.* (Preprint on Arxiv, `https://doi.org/10.48550/arXiv.2310.12382`) doi: 10.48550/arXiv.2310.12382

de Kleer, K., McEwen, A. S., Park, R. S., Bierson, C. J., Davies, A. G., DellaGiustina, D. N., ... Schneider, N. M. (2019). *Tidal heating: Lessons from Io and the Jovian system.* Final Report for the Keck Institute for Space Studies.

Gyalay, S., & Nimmo, F. (2023a). Estimates for Tethys' moment of inertia, heat flux distribution, and interior structure from its long-wavelength topography. *Journal of Geophsyical Research: Planets*, *128*(2). doi: 10.1029/2022JE007550

Gyalay, S., & Nimmo, F. (2023b). *Isostatic response of io's topography to the spatial variation of its tidal heating.* Dataset. Dryad. Retrieved from `https://datadryad.org/stash/share/YOzgrXbQG_GixJeSwZfZU98JdovcqvV1yJYAZGPZLhw` (This is a private URL for peer review. The repository will be made public with a doi for the final draft.)

Hamilton, C. W., Beggan, C. D., Still, S., Beuthe, M., Lopes, R. M. C., Williams, D. A., ... Wright, W. (2013). Spatial distribution of volcanoes on Io: Implications for tidal heating and magma ascent. *Earth and Planetary Science Letters*, *361*, 272–286. doi: 10.1016/j.epsl.2012.10.032

Hay, H., & Matsuyama, I. (2019). Nonlinear tidal dissipation in the subsurface oceans of Enceladus and other icy satellites. *Icarus*, *319*, 68–85. doi: 10.1016/j.icarus.2018.09.019

Hemingway, D., & Masuyama, I. (2017). Isostatic equilibrium in spherical coordinates and implications for crustal thickness on the Moon, Mars, Enceladus, and elsewhere. *Geophysical Research Letters*, *44*(15), 7695–7705. doi: 10.1002/2017GL073334

Jaeger, W. L., Turtle, E. P., Keszthelyi, L. P., Radebaugh, J., McEwen, A. S., & Pappalardo, R. T. (2003). Orogenic tectonism on Io. *Journal of Geophysical Research: Planets*, *108*(E8). doi: 10.1029/2002JE001946

Keane, J. T., de Kleer, K., & Spencer, J. (2022). Perspective: the future exploration of Io. *Elements*, *18*(6), 399–404. doi: 10.2138/gselements.18.6.399

Keszthelyi, L., & McEwen, A. (1997). Magmatic differentiation of Io. *Icarus*, *130*(2), 437–448. doi: 10.1006/icar.1997.5837

Khurana, K. K., Jia, X., Kivelson, M. G., Nimmo, F., Schuber, G., & Russell, C. T. (2011). Evidence of a global magma ocean in Io's interior. *Science*, *332*(6034), 1186–1189. doi: 10.1126/science.1201425

Lainey, V., Arlot, J., Karatekin, O., & Van Hoolst, T. (2009). Strong tidal dissipation in Io and Jupiter from astrometric observations. *Nature*, *459*, 957–959. doi: 10.1038/nature08108

Matusyama, I. N., Steinke, T., & Nimmo, F. (2022). Tidal heating in Io. *Elements*, *18*(6), 374–378. doi: 10.2138/gselements.18.6.374

McEwen, A. S., Keszthelyi, L. P., Lopes, R., Schenk, P. M., & Spencer, J. R. (2004). Jupiter: The planet, satellites and magnetosphere. In F. Bagenal, T. E. Dowling, & W. B. McKinnon (Eds.), (pp. 307–328). Cambridge University Press.

McKenzie, D., Nimmo, F., Jackson, J. A., Gans, P. B., & Miller, E. L. (2000). Characteristics and consequences of flow in the lower crust. *Journal of Geophysical Research: Solid Earth*, *105*, 11029–11046. doi: 10.1029/1999JB900446

Miyazaki, Y., & Stevenson, D. J. (2022). a subsurface magma ocean on Io: exploring the steady state of partially molten planetary bodies. *Planetary Science Journal*, *3*(11), 256. doi: 10.3847/PSJ/ac9cd1

Nash, D., Yoder, C., Carr, M., Gradie, J., & Hunten, D. (1986). Satellites. In J. A. Burns & M. S. Matthews (Eds.), (chap. Io: history of studies and current level of understanding of this satellite). University of Arizona Press.

Nimmo, F. (2004). Non-Newtonian topographic relaxation on Europa. *Icarus*, *168*(1), 205–208. doi: 10.1016/j.icarus.2003.11.022

Nimmo, F., & Stevenson, D. J. (2001). Estimates of Martian crustal thickness from viscous relaxation of topography. *Journal of Geophysical Research: Planets*, *106*(E3), 5085–5098. doi: 10.1029/2000JE001331

O'Reilly, T. C., & Davies, G. F. (1981). Magma transport of heat on Io: A mechanism allowing a thick lithosphere. *Geophysical Research Letters*, *8*(4), 313–316. doi: 10.1029/GL008i004p00313

Peale, S. J., Cassen, P., & Reynolds, R. T. (1979). Melting of Io by tidal dissipation. *Science*, *203*(4383), 892–894. doi: 10.1126/science.203.4383.892

Pettine, M., Imbeah, S., Rathbun, J., Hayes, A., Lopes-Gautier, R., Mura, A., ... Bertolino, S. (2023). *JIRAM observations of volcanic flux on Io: Distribution and comparison to tidal heat flow models.* (Preprint on Arxiv, `https://doi.org/10.48550/arXiv.2308.05717`) doi: 10.48550/arXiv.2308.05717

Rathbun, J. A., Spencer, J. R., Lopes, R. M., & Howell, R. R. (2014). Io's active volcanoes during the New Horizons era: insights from New Horizons imaging. *Icarus*, *231*, 261–272. doi: 10.1016/j.icarus.2013.12.002

Rathbun, J. A., Spencer, J. R., Tamppari, L. K., Martin, T. Z., Barnard, L., & Travis, L. D. (2004). Mapping of Io's thermal radiation by the Galileo photopolarimeter-radiometer (PPR) instrument. *Icarus*, *169*(1), 127–139. doi: 10.1016/j.icarus.2003.12.021

Schenk, P., Hargitai, H., Wilson, R., McEwen, A., & Thomas, P. (2001). The mountains of Io: Global and geological perspectives from Voyager and Galileo. *Journal of Geophysical Research: Planets*, *106*(E12), 33201–33222. doi: 10.1029/2000JE001408

Schubert, G., Anderson, J. D., Spohn, T., & McKinnon, W. B. (2004). Jupiter: the planet, satellites, and magnetosphere. In F. Bagenal, T. E. Dowling, & W. B. McKinnon (Eds.), (Vol. 2, p. 281). Cambridge University Press.

Segatz, M., Spohn, T., Ross, M. N., & Schubert, G. (1988). Tidal dissipation, surface heat flow, and figure of viscoelastic models of io. *Icarus*, *75*(2), 187–206. doi: 10.1016/0019-1035(88)90001-2

Simonelli, D. P., Dodd, C., & Veverka, J. (2001). Regolith variations on Io: Implications for bolometric albedos. *Journal of Geophysical Research: Planets*, *106*(E12), 33241–33252. doi: 10.1029/2000JE001350

Soderlund, K. (2019). Ocean dynamics of outer solar system satellites. *Geophysical Research Letters*, *46*(15), 8583–9299. doi: 10.1029/2018GL081880

Soderlund, K., Lemasquerier, D., & Bierson, C. (2023). Europa's ocean translates interior tidal heating patterns to the ice-ocean boundary. In *53rd Lunar and Planetary Science Conference.*

Spencer, D. C., Katz, R. F., & Hewitt, I. J. (2021). Tidal controls on the lithospheric thickness and topography of Io from magmatic segregation and volcanism modelling. *Icarus*(in press). doi: 10.1016/j.icarus.2021.114352

Steinke, T., Hu, H., Höning, D., van der Wal, W., & Vermeersen, B. (2020a). Tidally induced lateral variations of Io's interior. , *335*. doi: 10.1016/j.icarus.2019.05.001

Steinke, T., van Sliedregt, D., Vilella, K., van der Wal, W., & Vermeersen, B. (2020b). Can a combination of convective and magmatic heat transport in the mantle explain Io's volcanic pattern? *Journal of Geophysical Research: Planets*, *125*(12). doi: 10.1029/2020JE006521

Tackley, P. J. (2001). Convection in Io's asthenosphere: redistribution of nonuniform tidal heating by mean flows. *Journal of Geophysical Research: Planets*, *106*(E12), 32971–32981. doi: 10.1029/2000JE001411

Tackley, P. J., Schubert, G., Glatzmaier, G. A., Schenk, P., Ratcliff, J. T., & Matas, J.-P. (2001). Three-dimensional simulations of mantle convection in Io. *Icarus*, *149*(1), 79-93. doi: 10.1006/icar.2000.6536

Turcotte, D., & Schubert, G. (2014). *Geodynamics* (3rd ed.). Cambridge University Press, Cambridge (UK).

Tyler, R. H., Henning, W. G., & Hamilton, C. W. (2015). Tidal heating in a magma ocean within Jupiter's moon Io. *The Astrophysical Journal*, *218*(2), 22. doi: 10.1088/0067-0049/218/2/22

Veeder, G. J., Matson, D. L., Johnson, T. V., Blaney, D. L., & Goguen, J. D. (1994). Io's heat flow from infrared radiometry: 1983-1993. *Journal of Geophysical Research: Planets*, *99*, 17095–17162. doi: 10.1029/94JE00637

Supporting Information for "Io's Long Wavelength Topography as a Probe for a Subsurface Magma Ocean"

S. Gyalay[1]and F. Nimmo[1]

[1]University of California, Santa Cruz

Contents of this file

1. Text S1 to S2
2. Table S1

Introduction This supplement expands on points raised in the main paper, but that were not necessarily the focus of that paper. Section S1 details a calculation of the minimum thickness of Io's lithosphere needed to support its mountains. Section S2 shows the mismatch in Io's observed global shape, and that which one expects from a satellite in hydrostatic equilibrium. Table S1 accompanies Section S2.

Text S1. Minimum Thickness of Io's Lithosphere

Assuming Io's heat flow was dominated entirely by thermal conduction, a minimum heat flow of $F = 2$ W m^{-2} (Veeder et al., 1994; Simonelli et al., 2001; McEwen et al., 2004; Rathbun et al., 2004; de Kleer et al., 2019) would imply a lithosphere only 2.25 km thick (assuming constants in Table 1 of the main text). Yet Io's landscape includes mountains $\sim$ 10 km high (Carr et al., 1979, 1998; Schenk et al., 2001). Assuming a floating elastic lithopshere 5 km thick, O'Reilly and Davies (1981) calculated a mountain 10 km high and 10 km wide would generate a maximum bending stress of 6 kbar (60 MPa), while the strength of Earth's lithosphere at low pressure was estimated to have a maximum of 1-2 kbar (10-20 MPa). This led to the conclusion that most of Io's heat was advected to to the surface via heat-pipe volcanism (O'Reilly & Davies, 1981). Repeating from the main text, O'Reilly and Davies (1981) describe the combined conductive and advective heatl flux through Io's lithosphere as,

$$F = v\rho\left[\Delta H_f + C_p\left(T_m - T_s\right)\right] + \frac{v\rho C_p\left(T_m - T_s\right)}{e^{vd/\kappa} - 1}, \tag{1}$$

where v is the resurfacing rate, ρ is the magma density, ΔH_f is the latent heat of fusion, C_p is the specific heat, T_m is the melting temperature, T_s is the surface temperature, κ is the thermal diffusivity, and d the lithospheric thickness. Under Equation 1, the lithosphere could have an arbitrarily high thickness when the volcanic emplacement rate is high.

In order to qualify our predictions for long-wavelength topography as a result of tidal heat flux variations (Section 3 of the main text), it would help to have a minimum lithosphere thickness as a point of comparison. Carr et al. (1998) find the lower limit of 30 km set forth by Nash, Yoder, Carr, Gradie, and Hunten (1986) to be reasonable, even if "the origin of this 30-km number was obscure." By modeling the magmatic differentiation of Io, Keszthelyi and McEwen (1997) estimate a lithosphere thickness of 50 km. Then Jaeger et al. (2003) estimate that the minimum lithosphere thickness to support the volume of every mountain on Io is 12 km.

We revisit the method used by O'Reilly and Davies (1981) to formulate our own estimate of minimum lithosphere thickness. O'Reilly and Davies (1981) cite McNutt (1980), but the same approach is covered in Walcott (1976); Banks, Parker, and Huestis (1977); Turcotte and Schubert (2014). Imagine an elastic lithosphere of thickness d. In response to some line-load P at $x = 0$ (where x is a horizontal coordinate along the surface of the lithosphere), there will be a deflection $w(x)$ (where w is positive downward, beneath the undeflected surface) such that

$$D\frac{d^4 w}{dx^4} + \Delta\rho g w = 0, \tag{2}$$

where $\Delta\rho$ is the density contrast between the crustal (lithospheric, in our approximation) density ρ_c and mantle density ρ_m, g is gravitational acceleration, and D is the flexural rigidity of the lithosphere, defined

$$D = \frac{Ed^3}{12\left(1-\nu^2\right)}, \tag{3}$$

for the Young's Modulus E and Poisson's Ratio ν of the lithosphere (e.g., Walcott, 1976; Banks et al., 1977; Turcotte & Schubert, 2014). The maximum bending stress experienced by the lithosphere is

$$\sigma_{max} = -Ez\frac{d^2 x}{dx^2}, \tag{4}$$

where z is depth below the midway point of the lithosphere (i.e., σ_{max} at the base of the lithosphere is at $z = d/2$; Walcott, 1976). In response to a line load P, one can find the maximum curvature of the lithosphere

$$\left.\frac{d^2 w}{dx^2}\right|_{x=0} = -\frac{2w_0}{\alpha^2}, \tag{5}$$

where w_0 is w at $x = 0$ and the flexural parameter α is defined

$$\alpha^4 = \frac{4D}{\Delta\rho g}, \tag{6}$$

(Walcott, 1976). The maximum deflection w_0 in response to a line-load P is

$$w_0 = \frac{P\alpha^3}{8D}, \tag{7}$$

following Turcotte and Schubert (2014).

Combining the preceding equations, we find the maximum bending stress experienced at the base of a floating, elastic lithosphere under a line-load $P = \rho_c g h \lambda$ (where h is the height and λ is the half-width of the infinitely long line-load) is

$$\sigma_{max} = \frac{1}{8}\rho_c h\lambda \left\{ \frac{4E\left[12g\left(1-\nu^2\right)\right]^3}{\Delta\rho d^5} \right\}^{1/4}, \tag{8}$$

where one can see that the larger the lithosphere thickness d is, the lower the maximum bending stress at the base of the lithosphere is.

As O'Reilly and Davies (1981) did not provide the exact equations they used in their estimation, we double check our formulae against their result ($\sigma_{max} = 6$ kbar) to be sure that we are solving for the right value. Following O'Reilly and Davies (1981), for a 10 km high mountain that is 10 km wide ($\lambda = 5$ km) under Io gravity $g = 1.8$ m s^{-2} on a floating, elastic lithosphere with thickness $d = 5$ km, Young's Modulus $E = 80$ GPa, Poisson's ratio $\nu = 0.25$, $\rho_c = 3000$ kg m^{-3}, and density contrast with the mantle $\Delta\rho = 500$ kg m^{-3}; we find a maximum bending stress of 6.75 kbar. This is marginally larger than O'Reilly and Davies (1981)'s estimate, but that may have resulted from a difference in the assumed Young's Modulus or the assumed geometry of the surface load.

Satisfied that we are on the same track as O'Reilly and Davies (1981), we can now solve for the minimum lithosphere thickness that can support the observed topography on Io, where $\sigma_{max} < 2$ kbar. All else held constant for the assumed physical parameters of Io's lithosphere, Equation 8 reduces to

$$\sigma_{max} = 6.75\text{kbar} \times \left(\frac{5\text{km}}{d}\right)^{5/4}. \tag{9}$$

We then invert the equation to solve for d given $\sigma_{max} < 2$ kbar, and find a minimum lithosphere thickness $d > 23$ km.

Text S2. The Global Shape of Io

The shape $H(\theta, \lambda)$ of nearly-spherical bodies such as satellites can be described as function of the distance between the satellite's surface from its center of mass as a function of colatitude θ ($\frac{\pi}{2}$ subtracted by the latitude, where Northern latitudes are positive) and longitude λ (where East is positive). As a surface defined in spherical coordinates, one may then describe the shape using spherical harmonics. Here, some function $f(\theta, \lambda)$ is the sum of spherical harmonics with coefficients $C_{l,m}$ and $S_{l,m}$ for each degree l and order m,

$$f(\theta, \lambda) = \sum_{l=0}^{\infty} \sum_{m=0}^{l} \left(C_{l,m} \cos m\lambda + S_{l,m} \sin m\lambda\right) P_{l,m}(\cos\theta), \tag{10}$$

where $P_{l,m}(\cos\theta)$ is an associated Legendre function (e.g. Blakely, 1995). The spherical harmonic degree l indicates the length-scale (or wavelength) over which some value oscillates across a sphere. This wavelength is (approximately) the sphere's circumference divided by the degree l.

As tidal heating varies spatially in even orders of spherical harmonic degrees 2 and 4 (e.g. Beuthe, 2013), we use only those spherical harmonic coefficients of shape to isolate for the topography that could have arisen from variations in tidal heating. In this paper, we will refer to the spherical harmonic coefficients of shape as $H_{l,m}$. Spherical harmonic coefficients $H_{2,0}$ and $H_{2,2}$ may be calculated from the total triaxial shape of Io, which is

$$H^{tri}(\theta, \lambda) = \frac{1}{2} H_{2,0} \left(3\cos^2\theta - 1\right) + 3H_{2,2}\cos 2\lambda \sin^2\theta. \tag{11}$$

For a massive enough satellite, its self-gravity should ensure that the satellite adopts a practically spherical shape in hydrostatic equilibrium. Spinning bodies will become oblate due to rotational flattening. Further, because a satellite orbits a planet, the planet will raise a tidal bulge upon the satellite. When a satellite is in a synchronous orbit, there is an average, "permanent," bulge along the axis that points from the satellite to its host planet. Approximated as a triaxial ellipsoid, the length of each of a satellite's orthogonal axes can be denoted a, b, and c, where $a > b > c$ and a is the ellipsoid's largest possible axis. With the axes defined as such, a must then point from the satellite towards the planet ($\theta = \pi/2$, $\lambda = 0$), while c is the satellite's spin pole ($\theta = 0$), leaving b to point along the path of the satellite's orbit ($\theta = \pi/2$, $\lambda = \pi/2$). Thus, using these axes with Equation 11, one can calculate these spherical harmonic coefficients as $H_{2,0} = c - R_0$ and $H_{2,2} = (a - b)/6$. For Io, these axes a, b, and c are 1829.7, 1819.2, and 1815.8 km, respectively; with an error of 0.3 km (Thomas et al., 1998). With this measurement, we may then calculate the degree $l = 2$ terms of even order for Io's shape (Table S1).

Then, we calculate spherical harmonic coefficients of shape $H_{l,m}$ for degrees $l \geq 3$ and orders m for Io from limb profiles (Thomas et al., 1998; Nimmo & Thomas, 2013; White et al., 2014) (Table S1). We list only the terms for even orders of spherical harmonic degrees 2 and 4, as only those matter for inferring the tidal heating pattern. These spherical harmonic coefficients have not been normalized in any fashion (cf., Nimmo et al., 2011). The errors in degree $l = 2$ and $H_{4,0}$ topography are about an order of magnitude less than the coefficient, while errors in $H_{4,2}$ and $H_{4,4}$ are the same order as the coefficient.

To analyze any relationship between Io's topography and its spatial variations in tidal heating, we must first remove the contribution to its topography of this rotational flattening and tidal bulge. Due to the axial symmetry of both rotational flattening and the tidal bulge, we need only the cosine terms of Equation 10 in even orders of degree-2. The second-order approximation of a satellite's hydrostatic shape from the theory of figures that accounts for rapid rotation (i.e., a spin period of less than a few days, as derived by Beuthe et al., 2016) are defined as a function of the fluid Love number h_2^F (of order unity), such that

$$H_{2,0}^{hyd} = -\frac{5}{6}h_2^F R_0 q \left(1 + \frac{76}{105}h_2^F q\right), \tag{12}$$

$$H_{2,2}^{hyd} = \frac{1}{4}h_2^F R_0 q \left(1 + \frac{44}{21}h_2^F q\right), \tag{13}$$

where q is the ratio of rotational and gravitational forces, $q = \frac{\omega^2 R_0^3}{GM}$ (cf., Zharkov & Gudkova, 2010; Tricarico, 2014). By dropping the higher order term within the parentheses, the ratio $-H_{2,0}^{hyd}/H_{2,2}^{hyd}$ can readily be calculated as its first order approximation, 10/3. Because the term $H_{2,2}^{hyd}$ has a greater second-order increase compared respectively to the second-order increase of $H_{2,0}^{hyd}$, the actual ratio $-H_{2,0}^{hyd}/H_{2,2}^{hyd}$ will shrink from 10/3. We include the higher order terms for completeness but find they are insignificant for Io, as $q = 0.0017$.

For a hydrostatic body, the fluid Love number h_2^F is related to the body's mean moment of inertia C (a measure of mass distribution) by the Darwin-Radau relation (e.g. Munk

& MacDonald, 1960),

$$h_2^F = \frac{5}{1 + \left[\frac{5}{2}\left(1 - \frac{3}{2}\frac{C}{MR_0^2}\right)\right]^2}, \tag{14}$$

where the moment of inertia has been normalized by the satellite's mass M and mean radius R_0 squared. The normalized moment of inertia for a sphere of uniform density is $0.4\ MR_0^2$, and lower if more mass is concentrated in the core. For Io, we know its moment of inertia to be $0.3782MR_0^2$ from gravity measurements assuming it is in hydrostatic equilibrium (Schubert et al., 2004), thus finding $h_2^F = 2.3$ using Equation 14. This allows us to calculate Io's hydrostatic shape as $H_{2,0}^{hyd} = -5.95$ km and $H_{2,2}^{hyd} = 1.80$ km. Unfortunately, this means that when we eliminate the hydrostatic contribution to Io's shape, the remaining topography relative to the hydrostatic shape (and thus the topography we would assume is due to isostatic variations) is only $H_{2,0}^{rem} = 0.15$ km and $H_{2,2}^{rem} = 0.05$ km, which is less than the error in degree-2 topography (Table S1). Thus, it is unlikely we could make any conclusion on Io's tidal heating pattern from its global shape.

References

Banks, R. J., Parker, R. L., & Huestis, S. P. (1977). Isostatic compensation on a continental scale: local versus regional mechanisms. *Geophysical Journal International*, *51*(2), 431–452. doi: 10.1111/j.1365-246X.1977.tb06927.x

Beuthe, M. (2013). Spatial patterns of tidal heating. *Icarus*, *223*(1), 308–329. doi: 10.1016/j.icarus.2012.11.020

Beuthe, M., Rivoldini, A., & Trinh, A. (2016). Enceladus's and dione's flating ice shells supported by minimum stress isostasy. *Geophysical Research Letters*, *43*(19), 10088–10096. doi: 10.1002/2016GL070650

Blakely, R. J. (1995). *Potential theory in gravity and magnetic applications.* Cambridge University Press, Cambridge (UK).

Carr, M. H., Masursky, H., Strom, R. G., & Terrile, R. J. (1979). Volcanic features of Io. *Nature*, *280*(5725), 729–733. doi: 10.1038/280729a0

Carr, M. H., McEwen, A. S., Howard, K. A., Chuang, F. C., Thomas, P., Schuster, P., ... Galileo Imaging Team (1998). Mountains and calderas on Io: Possible implications for lithosphere structure and magma generation. *Icarus*, *135*(1), 146–165. doi: 10.1006/icar.1998.5979

de Kleer, K., McEwen, A. S., Park, R. S., Bierson, C. J., Davies, A. G., DellaGiustina, D. N., ... Schneider, N. M. (2019). *Tidal heating: Lessons from Io and the Jovian system.* Final Report for the Keck Institute for Space Studies.

Jaeger, W. L., Turtle, E. P., Keszthelyi, L. P., Radebaugh, J., McEwen, A. S., & Pappalardo, R. T. (2003). Orogenic tectonism on Io. *Journal of Geophysical Research: Planets*, *108*(E8). doi: 10.1029/2002JE001946

Keszthelyi, L., & McEwen, A. (1997). Magmatic differentiation of Io. *Icarus*, *130*(2), 437–448. doi: 10.1006/icar.1997.5837

McEwen, A. S., Keszthelyi, L. P., Lopes, R., Schenk, P. M., & Spencer, J. R. (2004). Jupiter: The planet, satellites and magnetosphere. In F. Bagenal, T. E. Dowling, & W. B. McKinnon (Eds.), (pp. 307–328). Cambridge University Press.

McNutt, M. (1980). Implications of regional gravity for state of stress in the Earth's crust and upper mantle. *Journal of Geophysical Research: Solid Earth*, *85*(B11), 6377–6396. doi: 10.1029/JB085iB11p06377

Munk, W. H., & MacDonald, G. J. F. (1960). *The rotation of the earth: a geophysical discussion.* Cambridge University Press, Cambridge (UK).

Nash, D., Yoder, C., Carr, M., Gradie, J., & Hunten, D. (1986). Satellites. In J. A. Burns & M. S. Matthews (Eds.), (chap. Io: history of studies and current level of understanding of this satellite). University of Arizona Press.

Nimmo, F., Bills, B. G., & Thomas, B. C. (2011). Geophysical implications of the long-wavelength topography of the Saturnian satellites. *Journal of Geophysical Research*, *116*, E11001. doi: 10.1029/2011JE003835

Nimmo, F., & Thomas, P. C. (2013). Geophysical implications of Io limb profile data. In *American geophysical union fall meeting 2013.*

O'Reilly, T. C., & Davies, G. F. (1981). Magma transport of heat on Io: A mechanism allowing a thick lithosphere. *Geophysical Research Letters*, *8*(4), 313–316. doi: 10.1029/GL008i004p00313

Rathbun, J. A., Spencer, J. R., Tamppari, L. K., Martin, T. Z., Barnard, L., & Travis, L. D. (2004). Mapping of Io's thermal radiation by the Galileo photopolarimeter-radiometer (PPR) instrument. *Icarus*, *169*(1), 127–139. doi: 10.1016/j.icarus.2003.12.021

Schenk, P., Hargitai, H., Wilson, R., McEwen, A., & Thomas, P. (2001). The mountains of Io: Global and geological perspectives from Voyager and Galileo. *Journal of Geophysical Research: Planets*, *106*(E12), 33201–33222. doi: 10.1029/2000JE001408

Schubert, G., Anderson, J. D., Spohn, T., & McKinnon, W. B. (2004). Jupiter: the planet, satellites, and magnetosphere. In F. Bagenal, T. E. Dowling, & W. B. McKinnon (Eds.), (Vol. 2, p. 281). Cambridge University Press.

Simonelli, D. P., Dodd, C., & Veverka, J. (2001). Regolith variations on Io: Implications for bolometric albedos. *Journal of Geophysical Research: Planets*, *106*(E12), 33241–33252. doi: 10.1029/2000JE001350

Thomas, P. C., Davies, M. E., Colvin, T. R., Oberst, J., Schuster, P., Neukum, G., … Team, G. I. (1998). The shape of Io from Galileo limb measurements. *Icarus*, *135*, 175–180. doi: 10.1006/icar.1998.5987

Tricarico, P. (2014). Multi-layer hydrostatic equilibrium of planets and synchronus moons: theory and application to Ceres and to solar system moons. *The Astrophysical Journal*, *782*(2), 99. doi: 10.1088/0004-637X/782/2/99

Turcotte, D., & Schubert, G. (2014). *Geodynamics* (3rd ed.). Cambridge University Press, Cambridge (UK).

Veeder, G. J., Matson, D. L., Johnson, T. V., Blaney, D. L., & Goguen, J. D. (1994). Io's heat flow from infrared radiometry: 1983-1993. *Journal of Geophysical Research: Planets*, *99*, 17095–17162. doi: 10.1029/94JE00637

Walcott, R. I. (1976). Geophysics of the pacific ocean basin and its margin. In G. H. Sutton, M. H. Manghnani, R. Moberly, & E. U. Mcafee (Eds.), (chap. Lithospheric Flexure, Analysis of gravity anomalies, and the propagation of seamount chains). American Geophysical Union. doi: 10.1029/GM019p0431

White, O. L., Schenk, P. M., Nimmo, F., & Hoogenboom, T. (2014). A new stereo topographic map of Io: implications for geology from global to local scales. *Journal of Geophysical Research: Planets*, *119*(6), 1276–1301. doi: 10.1002/2013JE004591

Zharkov, V., & Gudkova, T. (2010). Models, figures, and gravitational moments of Jupiter's satellite Io: effects of the second order approximation. *Planetary and Space Science*, *58*(10), 1381–1390. doi: 10.1016/j.pss.2010.06.004

Table S1. Spherical harmonic coefficients of Io's shape[a]

l	m	$H_{l,m}$ (km)		$\sigma_{Hl,m}$ (km)
2	0	-5.8	$\pm$	0.4
2	2	1.7	$\pm$	0.1
4	0	-0.06	$\pm$	0.02
4	2	-0.0016	$\pm$	0.0016
4	4	-0.00016	$\pm$	0.00016

[a] $l = 2$ terms were calculated with Equation 11, while $l = 4$ terms were calculated with the method of White et al. (2014) using smoothing parameter $r = 3 \times 10^7$. These terms are not normalized.